Eur. Phys. J. C 33, 349–368 (2004)
Digital Object Identifier (DOI) 10.1140/epjc/s2004-01592-0

THE EUROPEAN PHYSICAL JOURNAL C

Exclusive $B \to (K^*, \rho)\gamma$ decays in general two-Higgs-doublet models

Zhenjun Xiao[1,2,a], Ci Zhuang[3]

[1] Department of Physics, Nanjing Normal University, Nanjing, Jiangsu 210097, P. R. China
[2] CCAST (World Laboratory), P. O. Box 8730, Beijing 100080, P. R. China
[3] Department of Physics, Nanjing Normal University, Nanjing, Jiangsu 210097, P. R. China

Received: 9 October 2003 / Revised version: 11 November 2003 /
Published online: 18 February 2004 –

Abstract. By employing the QCD factorization approach, we calculated the next-to-leading order new physics contributions to the branching ratios, CP asymmetries, isospin and U-spin symmetry breaking of the exclusive decays $B \to V\gamma$ ($V = K^*, \rho$), induced by the charged Higgs penguins in general two-Higgs-doublet models. Within the considered parameter space, we found that (a) the new physics corrections to the observables are generally small in model I and model III-A, moderate in model II, but large in model III-B; (b) from the well measured branching ratios and upper limits, a lower bound of $M_H > 200\,\mathrm{GeV}$ in model II was obtained, while the allowed range of M_H in model III-B is $226 \le M_H \le 293\,\mathrm{GeV}$; these bounds are comparable with those from the inclusive $B \to X_s\gamma$ decay; (c) the NLO Wilson coefficient $C_7(m_b)$ in model III-B is positive and disfavored by the measured value of isospin symmetry breaking $\Delta_{0-}^{\mathrm{exp}}(K^*\gamma) = (3.9 \pm 4.8)\%$, but it still cannot be excluded if we take the large errors into account; (d) the CP asymmetry $\mathcal{A}_{CP}(B \to \rho\gamma)$ in model III-B has an opposite sign to the one in the standard model (SM), which may be used as a good observable to distinguish the SM from model III-B; (e) the isospin symmetry breaking $\Delta(\rho\gamma)$ is less than 10% in the region of $\gamma = [40 \sim 70]^\circ$ preferred by the global fit result, but it can be as large as 20 to 40% in the regions of $\gamma \le 10^\circ$ and $\gamma \ge 120^\circ$. The SM and model III-B predictions for $\Delta(\rho\gamma)$ are opposite in sign for small or large values of the CKM angles; (f) the U-spin symmetry breaking $\Delta U(K^*, \rho)$ in the SM and the general two-Higgs-doublet models is generally small in size: $\sim 10^{-7}$.

1 Introduction

As is well known, the inclusive radiative decays $B \to X_q\gamma$ with $q = (d, s)$ and the corresponding exclusive decays $B \to V\gamma$ ($V = K^*, \rho$) are very sensitive to the flavor structure of the standard model (SM) and to the new physics models beyond the SM and have been studied in great detail by many authors [1–3].

For the inclusive $B \to X_s\gamma$ decay mode, the world average of the branching ratio [4] is

$$\mathcal{B}(B \to X_s\gamma) = (3.34 \pm 0.38) \times 10^{-4}\,, \qquad (1)$$

which agrees perfectly with the SM theoretical prediction at the next-to-leading order (NLO) [5–9] and puts perhaps most stringent bounds on many new physics models [10–13] where new particles such as the charged Higgs bosons may provide significant contributions through flavor changing loops.

The exclusive decay $B \to K^*\gamma$ has a very clean experimental signal and a low background, which was first observed by CLEO in 1992 [14], and measured recently by BaBar and Belle with good precision [15, 16]: the world averages of the CP-averaged branching ratios are [17]

$$\mathcal{B}(B \to \overline{K}^{*0}\gamma) = (4.17 \pm 0.23) \times 10^{-5},$$
$$\mathcal{B}(B \to K^{*-}\gamma) = (4.18 \pm 0.32) \times 10^{-5}\,, \qquad (2)$$

and they have reached a statistical accuracy of better than 10%. The measurements of the Cabibbo suppressed $B \to (\rho, \omega)\gamma$ decays are difficult because the signal is about 20 times smaller, and the continuum background is about 3 times larger than the $B \to K^*\gamma$ decay mode. Consequently, experiments have so far provided only upper bounds [14–16], but they will surely be measured at B factories in the near future. The currently available data as presented at the LP'2003 conference [17] are summarized in Table 1.

When compared with the inclusive $B \to X_{s,d}\gamma$ decays, the corresponding exclusive $B \to V\gamma$ decays are experimentally more tractable (specifically for the $B \to \rho\gamma$ mode) but theoretically less clean, since the bound state effects are essential and need to be described by some non-perturbative quantities like form factors and light-cone distribution amplitudes (LCDAs).

In [18–20], the branching ratios and rate asymmetries of $B \to V\gamma$ decays were investigated in leading order

[a] e-mail: xiaozhenjun@pine.njnu.edu.cn

Table 1. Experimental measurements of the CP-averaged branching ratios and/or CP violating asymmetries A_{CP} (at 90%$C.L.$) of the exclusive $B \to V\gamma$ decays for $V = K^*, \rho$ and ω

Channel	CLEO [14]	BaBar [15]	Belle [16]	Average
$\mathcal{B}(B \to K^{*0}\gamma)$ (10^{-5})	$4.55 \pm 0.70 \pm 0.34$	$4.23 \pm 0.40 \pm 0.22$	$4.09 \pm 0.21 \pm 0.19$	4.17 ± 0.23
$\mathcal{B}(B \to K^{*+}\gamma)$ (10^{-5})	$3.76 \pm 0.86 \pm 0.28$	$3.83 \pm 0.62 \pm 0.22$	$4.40 \pm 0.33 \pm 0.24$	4.18 ± 0.32
$\mathcal{B}(B \to \rho^0\gamma)$ (10^{-6})	< 17	< 1.2	< 2.6	
$\mathcal{B}(B \to \rho^+\gamma)$ (10^{-6})	< 13	< 2.1	< 2.7	
$\mathcal{B}(B \to \omega\gamma)$ (10^{-6})		< 1.0	< 4.4	
$\mathcal{A}_{CP}(B \to K^{*0}\gamma)$ (%)	$8 \pm 13 \pm 3$	$-3.5 \pm 9.4 \pm 2.2$	$-6.1 \pm 5.9 \pm 1.8$	
$\mathcal{A}_{CP}(B \to K^{*+}\gamma)$ (%)			$+5.3 \pm 8.3 \pm 1.6$	

(LO) and next-to-leading order (NLO) by employing the constituent quark model (CQM) [18]. In [21], the exclusive $B \to K^*\gamma$ decay was studied by using the perturbative QCD approach. Very recently, in the heavy quark limit $m_b \gg \Lambda_{\rm QCD}$, the decay amplitudes for the exclusive $B \to (K^*, \rho)\gamma$ decay modes have been calculated in a model-independent way by using a QCD factorization approach [22–24], which is similar in spirit to the scheme developed earlier for the non-leptonic two-body decays of the B meson [25]. The NLO standard model predictions for the branching ratios, CP and isospin asymmetries, as well as the U-spin breaking effects for $B \to K^*\gamma$ and $B \to \rho\gamma$ decays are now available [22–24, 26, 27]. The new physics effects on isospin symmetry breaking and direct CP violation in $B \to \rho\gamma$ decay have also been studied recently in supersymmetric models [28].

In a previous paper, we calculated the NLO new physics contributions to the B^0-$\overline{B}^0$ mixing and the inclusive $B \to X_s\gamma$ decay from the charged Higgs loop diagrams in the third type of two-Higgs-doublet model (model III) and the conventional model II. In this paper, we calculate the new physics contributions to the branching ratios, CP asymmetries, and isospin and U-spin symmetry breaking of the exclusive radiative decays $B \to (K^*, \rho)\gamma$ in the framework of the general two-Higgs-doublet models, including the conventional models I and II, and model III. The QCD factorization method for exclusive $B \to V\gamma$ decays as presented in [22–24] will be employed in our calculations.

This paper is organized as follows. In Sect. 2, we describe the basic structures of the general two-Higgs-doublet models, give a brief review about the calculation of $B \to V\gamma$ at NLO in QCD factorization approach in the SM and present the needed analytical formulas for the calculation of Wilson coefficients and physical observables. In Sect. 3 and 4, we calculate the NLO new physics contributions to the $B \to K^*\gamma$ and $B \to \rho\gamma$ decay, respectively. The conclusions are included in the final section.

2 Theoretical framework

For the standard model part, we follow the procedure of [24] and use the formulas as presented in [24, 26]. The QCD factorization approach to the exclusive $B \to V\gamma$ decays was applied independently in [22–24] with some differences in the definition and explicit expressions of the functions. We adopt the analytical formulas in the SM as presented in [24, 26] in this paper, since more details can be found there.

In this section, we present the effective Hamiltonian and the relevant formulas for the exclusive decays $B \to V\gamma$ in the framework of the SM and the general two-Higgs-doublet models.

2.1 Effective Hamiltonian for inclusive $b \to s\gamma$ decay

In the framework of the SM, if we only take into account operators up to dimension 6 and put $m_s = 0$, the effective Hamiltonian for $b \to s\gamma$ transitions at the scale μ reads [24]

$$\mathcal{H}_{\rm eff} = \frac{G_{\rm F}}{\sqrt{2}} \sum_{p=u,c} \lambda_p^s \left[C_1 Q_1^p + C_2 Q_2^p + \sum_{j=3}^{8} C_j Q_j \right], \quad (3)$$

where $\lambda_p^q = V_{pq}^* V_{pb}$ for $q = (d, s)$ is the Cabibbo–Kobayashi–Maskawa (CKM) factor [29]. And the current–current, QCD penguin, electromagnetic and chromomagnetic dipole operators in the standard basis[1] are given by[2]

$$\begin{aligned}
Q_1^p &= (\bar{s}p)_{V-A}(\bar{p}b)_{V-A}\,, \\
Q_2^p &= (\bar{s_\alpha}p_\beta)_{V-A}(\bar{p_\beta}b_\alpha)_{V-A}\,, \\
Q_3 &= (\bar{s}b)_{V-A}\sum(\bar{q}q)_{V-A}\,, \\
Q_4 &= (\bar{s_\alpha}b_\beta)_{V-A}\sum(\bar{q_\beta}q_\alpha)_{V-A}\,, \\
Q_5 &= (\bar{s}b)_{V-A}\sum(\bar{q}q)_{V+A}\,, \\
Q_6 &= (\bar{s_\alpha}b_\beta)_{V-A}\sum(\bar{q_\beta}q_\alpha)_{V+A}\,, \\
Q_7 &= \frac{e}{8\pi^2} m_b \bar{s_\alpha}\sigma^{\mu\nu}(1+\gamma_5)b_\alpha F_{\mu\nu}\,, \\
Q_8 &= \frac{g}{8\pi^2} m_b \bar{s_\alpha}\sigma^{\mu\nu}(1+\gamma_5)T^a_{\alpha\beta}b_\beta G^a_{\mu\nu}\,, \qquad (4)
\end{aligned}$$

[1] There is another basis: the CMM basis, introduced by Chetyrkin, Mosiak, and Münz [5] where the fully anticommuting γ_5 in dimensional regularization are employed. The corresponding operators and Wilson coefficients in the CMM basis are denoted as P_i and Z_i in [24]. For more details see [5,26].

[2] For the numbering of operators $Q_{1,2}^p$, we use the same convention as [26] throughout this paper.

where T_a $(a = 1, \ldots, 8)$ stands for the $SU(3)_c$ generators, α and β are color indices, e and g_s are the electromagnetic and strong coupling constants, Q_1 and Q_2 are current–current operators, Q_3–Q_6 are the QCD penguin operators, Q_7 and Q_8 are the electromagnetic and chromomagnetic penguin operators. The effective Hamiltonian for $b \to d\gamma$ is obtained from (3) and (4) by the replacement $s \to d$.

To calculate the exclusive $B \to V\gamma$ decays complete to next-to-leading order in QCD and to leading order in $\Lambda_{\rm QCD}/M_B$, only the NLO Wilson coefficient $C_7(\mu_b)$ and LO Wilson coefficients $C_i(\mu_b)$ with $i = 1$–$6, 8$ and $\mu_b = \mathcal{O}(m_b)$ are needed. For the sake of the reader, we simply present these Wilson coefficients at the high matching scale M_W and the low energy scale $\mu_b = m_b$ here; one is referred to [1,5] for more details.

In the literature, one usually uses certain linear combinations of the original $C_i(\mu)$, the so-called "effective coefficients" $C^{\rm eff}(\mu)$ introduced in [5,30], in calculations. The corresponding transformations are of the form

$$C_i^{\rm eff}(\mu) = C_i(\mu) \quad (i = 1, \ldots, 6)\,, \tag{5}$$

$$C_7^{\rm eff}(\mu) = C_7(\mu) + \sum_{i=1}^{6} y_i C_i(\mu)\,, \tag{6}$$

$$C_8^{\rm eff}(\mu) = C_8(\mu) + \sum_{i=1}^{6} z_i C_i(\mu)\,, \tag{7}$$

with $\mathbf{y} = (0, 0, 0, 0, -1/3, -1)$ and $\mathbf{z} = (0, 0, 0, 0, 1, 0)$ in the NDR scheme [30], and $\mathbf{y} = (0, 0, -1/3, -4/9, -20/3, -80/9)$ and $\mathbf{z} = (0, 0, 1, 1/6, 20, -10/3)$ in the $\overline{\rm MS}$ scheme with fully anticommuting γ_5 [5]. In order to simplify the notation we will also omit the label "eff" throughout this paper.

Within the SM and at the matching scale $\mu = M_W$, the leading order Wilson coefficients are

$$C^0_{1,\rm SM}(M_W) = 1\,, \tag{8}$$

$$C^0_{i,\rm SM}(M_W) = 0, \quad i = 2, \ldots, 6\,, \tag{9}$$

$$C^0_{7,\rm SM}(M_W) = -\frac{A(x_t)}{2}\,, \tag{10}$$

$$C^0_{8,\rm SM}(M_W) = -\frac{D(x_t)}{2}\,, \tag{11}$$

with

$$A(x) = \frac{3x_t^3 - 2x_t^2}{4(x_t-1)^4}\ln x_t + \frac{-8x_t^3 - 5x_t^2 + 7x_t}{24(x_t-1)^3}\,, \tag{12}$$

$$D(x) = \frac{-3x_t^2}{4(x_t-1)^4}\ln x_t + \frac{-x_t^3 + 5x_t^2 + 2x_t}{8(x_t-1)^3}\,, \tag{13}$$

while the NLO results for $C_7(M_W)$ and $C_8(M_W)$ are

$$C^1_{7,\rm SM}(M_W) = \frac{-16x_t^4 - 122x_t^3 + 80x_t^2 - 8x_t}{9(x_t-1)^4}{\rm Li}_2\left(1 - \frac{1}{x_t}\right) + \frac{6x_t^4 + 46x_t^3 - 28x_t^2}{3(x_t-1)^5}\ln {x_t}^2 + \frac{-102x_t^5 - 588x_t^4 - 2262x_t^3 + 3244x_t^2 - 1364x_t + 208}{81(x_t-1)^5} \times \ln x_t + \frac{1646x_t^4 + 12205x_t^3 - 10740x_t^2 + 2509x_t - 436}{486(x_t-1)^4}\,, \tag{14}$$

$$C^1_{8,\rm SM}(M_W) = \frac{-4x_t^4 + 40x_t^3 + 41x_t^2 + x_t}{6(x_t-1)^4}{\rm Li}_2\left(1 - \frac{1}{x_t}\right) + \frac{-17x_t^3 - 31x_t^2}{2(x_t-1)^5}\ln {x_t}^2 + \frac{-210x_t^5 + 1086x_t^4 + 4893x_t^3 + 2857x_t^2 - 1994x_t + 208}{216(x_t-1)^5} \times \ln x_t + \frac{737x_t^4 - 14102x_t^3 - 28209x_t^2 + 610x_t - 508}{1296(x_t-1)^4}\,, \tag{15}$$

where $x_t = m_t^2/m_w^2$, and ${\rm Li}_2(x)$ is the dilogarithm function.

At the low energy scale $\mu = O(m_b)$, the leading order Wilson coefficients are

$$C^0_{j,\rm SM}(\mu) = \sum_{i=1}^{8} k_{ji}\eta^{a_i}, \quad \text{for} \quad j = 1, \ldots, 6\,, \tag{16}$$

$$C^0_{7,\rm SM}(\mu) = \eta^{\frac{16}{23}} C^0_{7,\rm SM}(M_W) + \frac{8}{3}\left(\eta^{\frac{14}{23}} - \eta^{\frac{16}{23}}\right) C^0_{8,\rm SM}(M_W) + \sum_{i=1}^{8} h_i \eta^{a_i}\,, \tag{17}$$

$$C^0_{8,\rm SM}(\mu) = C^0_{8,\rm SM}(M_W)\eta^{\frac{14}{23}} + \sum_{i=1}^{8} \hbar_8 \eta^{a_i} \tag{18}$$

in the standard basis, while

$$Z^0_{j,\rm SM}(\mu) = \sum_{i=1}^{8} h_{ji}\eta^{a_i}, \quad \text{for} \quad j = 1, \ldots, 6\,, \tag{19}$$

$$Z^0_{7,\rm SM}(\mu) = C^0_{7,\rm SM}(\mu)\,, \tag{20}$$

$$Z^0_{8,\rm SM}(\mu) = C^0_{8,\rm SM}(\mu) \tag{21}$$

in the CMM basis.

The NLO Wilson coefficient $C_7(\mu_b)$ at scale $\mu_b = \mathcal{O}(m_b)$ can be written as

$$C_{7,\rm SM}(\mu) = C^0_{7,\rm SM}(\mu) + \frac{\alpha_s(\mu)}{4\pi} C^1_{7,\rm SM}(\mu)\,, \tag{22}$$

with

$$C^1_{7,\rm SM}(\mu) = \eta^{\frac{39}{23}} C^1_{7,\rm SM}(M_W) + \frac{8}{3}\left(\eta^{\frac{37}{23}} - \eta^{\frac{39}{23}}\right) C^1_{8,\rm SM}(M_W) + \left(\frac{297664}{14283}\eta^{\frac{16}{23}} - \frac{7164416}{357075}\eta^{\frac{14}{23}} + \frac{256868}{14283}\eta^{\frac{37}{23}} - \frac{6698884}{357075}\eta^{\frac{39}{23}}\right) C^0_{8,\rm SM}(M_W)$$

Table 2. The "magic numbers" appearing in the calculations of the Wilson coefficients $C_i(\mu)$ in the rare decay $b \to q\gamma$ with $q = (d, s)$

i	1	2	3	4	5	6	7	8
a_i	$\frac{14}{23}$	$\frac{16}{23}$	$\frac{6}{23}$	$-\frac{12}{23}$	0.4086	−0.4230	−0.8994	0.1456
k_{1i}	0	0	$\frac{1}{2}$	$\frac{1}{2}$	0	0	0	0
k_{2i}	0	0	$\frac{1}{2}$	$-\frac{1}{2}$	0	0	0	0
k_{3i}	0	0	$-\frac{1}{14}$	$\frac{1}{6}$	0.0510	−0.1403	−0.0113	0.0054
k_{4i}	0	0	$-\frac{1}{14}$	$-\frac{1}{6}$	0.0984	0.1214	0.0156	0.0026
k_{5i}	0	0	0	0	−0.0397	0.0117	−0.0025	0.0304
k_{6i}	0	0	0	0	0.0335	0.0239	−0.0462	−0.0112
h_{1i}	0	0	1	−1	0	0	0	0
h_{2i}	0	0	$\frac{2}{3}$	$\frac{1}{3}$	0	0	0	0
h_{3i}	0	0	$\frac{2}{63}$	$-\frac{1}{27}$	−0.0659	0.0595	−0.0218	0.0335
h_{4i}	0	0	$\frac{1}{21}$	$\frac{1}{9}$	0.0237	−0.0173	−0.01336	−0.0136
h_{5i}	0	0	$-\frac{1}{126}$	$\frac{1}{108}$	0.0094	−0.01	0.001	−0.0017
h_{6i}	0	0	$-\frac{1}{84}$	$-\frac{1}{36}$	0.0108	0.0163	0.0103	0.0023
e_i	$\frac{4661194}{816831}$	$-\frac{8516}{2217}$	0	0	−1.9043	− 0.1008	0.01216	0.0183
f_i	−17.3023	8.5027	4.5508	0.7519	2.0040	0.7476	−0.5358	0.0914
g_i	14.8088	−10.809	−0.8740	0.4218	−2.9347	0.3971	0.1600	0.0225
h_i	2.2996	−1.0880	$-\frac{3}{7}$	$-\frac{1}{14}$	−0.6494	−0.0380	−0.0185	− 0.0057
$\hbar_i$	0.8623	0	0	0	−0.9135	0.0873	−0.0571	0.0209

Table 3. Values of the input parameters used in the numerical calculations [31–33]. For the value of F_{K^*}, we use the lattice QCD determination of $F_{K*} = 0.25 \pm 0.06$ [33] instead of the result $F_{K^*} = 0.38 \pm 0.06$ as given in [32]. The smaller value of F_{K^*} gives a better agreement between the SM predictions and the data. $R_b = \sqrt{\bar\rho^2 + \bar\eta^2}$, and $A, \lambda, \bar\rho$ and $\bar\eta$ are the ordinary Wolfenstein parameters of the CKM mixing matrix

A	λ	R_b	γ	$G_{\rm F}$	$\alpha_{\rm em}$
0.854	0.2196	0.39 ± 0.08	$(60 \pm 20)^\circ$	$1.1664 \times 10^{-5}\,\text{GeV}^{-2}$	1/137.036
$\alpha_{\rm s}(M_Z)$	m_W	m_t	$\Lambda^{(5)}_{\overline{\rm MS}}$	$m_c(m_b)$	m_u
0.119	80.42 GeV	174.3 GeV	225 MeV	1.3 ± 0.2 GeV	4.2 MeV
f_B	λ_B	m_{B_d}	$m_b(m_b)$	τ_{B^+}	τ_{B^0}
200 MeV	(350 ± 150) MeV	5.279 GeV	4.2 GeV	1.671 ps	1.537 ps
F_{K^*}	f_{K^*}	$f^\perp_{K^*}$	m_{K^*}	$\alpha_1^{K^*}$	$\alpha_2^{K^*}$
0.25 ± 0.06	230 MeV	185 MeV	894 MeV	0.2	0.04
F_ρ	f_ρ	$f^\perp_\rho$	m_ρ	α_1^ρ	α_2^ρ
0.29 ± 0.04	200 MeV	160 MeV	770 MeV	0	0.2

$$+\frac{37208}{4761}\left(\eta^{\frac{39}{23}}-\eta^{\frac{16}{23}}\right)C^0_{7,\rm SM}(M_W)$$
$$+\sum_{i=1}^{8}(e_i\eta E(x_t)+f_i+g_i\eta)\eta^{a_i}\,, \tag{23}$$

with

$$E(x)=\frac{x(x^2+11x-18)}{12(x-1)^3}+\frac{x^2(4x^2-16x+15)}{6(x-1)^4}\ln x$$
$$-\frac{2}{3}\ln x-\frac{2}{3}\,, \tag{24}$$

where $\eta = \alpha_{\rm s}(M_W)/\alpha_{\rm s}(\mu_b)$, and the "magic numbers" a_i, e_i, f_i, g_i, K_{ji} and h_{ji}, h_i and $\hbar_i$ are summarized in Table 2.

Using the central values of the input parameters as given in Table 3, we find the numerical results of the Wilson coefficients $C_i(m_b)$ and $Z_i(m_b)$ in the SM:

$$\overrightarrow{C^0}(m_b) = \{1.1167, -0.2670, 0.0120, -0.0274, 0.0078,$$
$$-0.0340, -0.3212, -0.1519\}\,, \tag{25}$$

$$\overrightarrow{Z^0}(m_b) = \{-0.5339, 1.0280, -0.0055, -0.0727, 0.0005,$$
$$0.0012, -0.3212, -0.1519\} \tag{26}$$

at the leading order, and

$$C_7(m_b) = \underbrace{-0.3212}_{C_7^0(m_b)} + \underbrace{0.0112}_{\Delta C_7^{\rm NLO}} = -0.3100 \tag{27}$$

at the next-to-leading order; the second term denotes the NLO QCD correction to $C_7^0(m_b)$.

2.2 $B \to V\gamma$ decay in the QCD factorization approach

Based on the effective Hamiltonian for the quark level process $b \to s(d)\gamma$, one can write down the amplitude for $B \to V\gamma$ and calculate the branching ratios and CP violating asymmetries once a method is derived for computing the hadronic matrix elements. One typical numerical result obtained by employing the constituent quark model [18] is

$$\mathcal{B}(B \to K^*\gamma) \approx 5 \times 10^{-5} \tag{28}$$

at both LO and NLO level [20]. Although this theoretical prediction is in good agreement with the data numerically, the hadronic models used in [18–20] did not allow a clear separation of short- and long-distance dynamics and a clean distinction of model-dependent and model-independent features. By using the QCD factorization approach [22–24], one can separate systematically perturbatively calculable hard-scattering kernels ($T_i^{\rm I}$ and $T_i^{\rm II}$) from non-perturbative form factors and universal light-cone distribution amplitudes of B, K^* and ρ mesons. The higher order QCD corrections can therefore be taken into account consistently.

In this paper, we calculate the new physics contributions to the exclusive decays $B \to K^*\gamma$ and $B \to \rho\gamma$ in the general two-Higgs-doublet models by employing the QCD factorization approach. We will always consider the decay widths or branching ratios averaged over the charge conjugated modes with the obvious exception of the CP asymmetries.

In the QCD factorization approach, the hadronic matrix elements of the operators Q_i with $i = 1, \ldots, 8$ for $B \to V\gamma$ decays can be written as [24]

$$\begin{aligned}&\langle V\gamma(\epsilon)|Q_i|\bar{B}\rangle \\ &= \left[F^{B\to V}(0)\, T_i^{\rm I} + \int_0^1 {\rm d}\xi\, {\rm d}v\, T_i^{\rm II}(\xi, v)\, \Phi_B(\xi)\, \Phi_V(v)\right] \cdot \epsilon\,,\end{aligned} \tag{29}$$

where ϵ is the photon polarization four-vector, $F^{B\to V}$ is the form factor describing $B \to V$ decays, Φ_B and Φ_V are the universal and non-perturbative light-cone distribution amplitudes for B and V meson respectively[3], $v\,(\bar{v} \equiv 1-v)$ is the momentum fraction of a quark (anti-quark) inside a light meson: $l_1^+ = vk^+$ and $l_2^+ = \bar{v}k^+$ while $k^\mu = (k^+, k^-, \mathbf{k}_\perp)$ is a four-vector in light-cone coordinates, ξ describes the momentum fraction of the light spectator quark inside a B meson: $l^+ = \xi p_B^+$ with $\xi = \mathcal{O}(\Lambda_{\rm QCD}/m_b)$, and $T_i^{\rm I}$ and $T_i^{\rm II}$ denote the perturbative short-distance interactions. The QCD factorization formula (29) holds up to corrections of relative order $\Lambda_{\rm QCD}/m_b$.

In the heavy quark limit, the contributions to the exclusive $B \to V\gamma$ decay can be classified into three classes[4].

(1) The "Type-I" or "hard vertex" contributions include (a) the contribution of the magnetic penguin operator Q_7 described by the form factor $F^{B\to V}$, which is the only contribution to the amplitude of $B \to V\gamma$ at the LO approximation, and (b) the $\mathcal{O}(\alpha_{\rm s})$ contribution to the hard-scattering kernels $T_i^{\rm I}$ from four-quark operators $Q_{1\ldots6}$ and the chromomagnetic penguin operator Q_8.
(2) The "Type-II" or "hard spectator" contributions include the $\mathcal{O}(\alpha_{\rm s})$ contribution to the hard-scattering kernels $T_i^{\rm II}$ from four-quark operators $Q_{1\ldots6}$ and the chromomagnetic penguin operator Q_8.
(3) The "Weak annihilation" contribution, which is suppressed by one power $\Lambda_{\rm QCD}/m_b$ when compared with the Type-I and -II contributions, and the dominant annihilation amplitudes can be computed within QCD factorization.

Combining all parts, the decay amplitude to $\mathcal{O}(\alpha_{\rm s})$ for exclusive $B \to V\gamma$ decay takes the form of

$$A(\overline{B} \to V\gamma) = \frac{G_{\rm F}}{\sqrt{2}} R_V \langle V\gamma|Q_7|\overline{B}\rangle\,, \tag{30}$$

with

$$\begin{aligned}R_V = {} & \lambda_u^{(q)}\, [a_7^u(V\gamma) + a_{\rm ann}^u(V\gamma)] \\ & + \lambda_c^{(q)}\, [a_7^c(V\gamma) + a_{\rm ann}^c(V\gamma)]\,,\end{aligned} \tag{31}$$

where $q = s$ for $V = K^*$, $q = d$ for $V = \rho$, and a_7^p $(p = u, c)$ denote the hard vertex and hard spectator NLO contributions

$$\begin{aligned}a_7^p(V\gamma) = {} & C_7(\mu) \\ & + \frac{\alpha_{\rm s}(\mu) C_F}{4\pi} \left[\sum_{i=1,2} Z_i^0(\mu) G_i(z_p) + \sum_{j=3\ldots6,8} Z_j^0(\mu) G_j\right] \\ & + \frac{\alpha_{\rm s}(\mu_h) C_F}{4\pi} \left[C_1^0(\mu_h) H_1^V(z_p) + \sum_{j=3\ldots6,8} C_j^0(\mu_h) H_j^V\right],\end{aligned} \tag{32}$$

where $z_q = m_q^2/m_b^2$, $\mu_h = \sqrt{0.5\mu}$, $C_F = 4/3$, the Wilson coefficients can be found in the previous subsection, and the explicit expressions of the functions G_i and H_j^V can be found in [26] and in Appendix A. The functions $a_{\rm ann}^u$ and $a_{\rm ann}^c$ in the above equation denote the weak annihilation contributions and take the form of [26]

$$\begin{aligned}a_{\rm ann}^u(\bar{K}^{*0}\gamma) &= Q_d \left[a_4 b^{K^*} + a_6 \left(d_v^{K^*} + d_{\bar{v}}^{K^*}\right)\right], \\ a_{\rm ann}^c(\bar{K}^{*0}\gamma) &= a_{\rm ann}^u(\bar{K}^{*0}\gamma), \\ a_{\rm ann}^u(K^{*-}\gamma) &= Q_u \left[a_1 b^{K^*} + a_4 b^{K^*} + a_6 \left(-2d_v^{K^*} + d_{\bar{v}}^{K^*}\right)\right], \\ a_{\rm ann}^c(K^{*-}\gamma) &= Q_u \left[a_4 b^{K^*} + a_6 \left(-2d_v^{K^*} + d_{\bar{v}}^{K^*}\right)\right]\end{aligned} \tag{33}$$

for $\overline{B} \to K^*\gamma$ decays, and

$$\begin{aligned}a_{\rm ann}^u(\rho^0\gamma) &= Q_d \left[-a_2 b^\rho + a_4 b^\rho + a_6 \left(d_v^\rho + d_{\bar{v}}^\rho\right)\right], \\ a_{\rm ann}^u(\rho^-\gamma) &= Q_u \left[a_1 b^\rho + a_4 b^\rho + a_6 \left(-2d_v^\rho + d_{\bar{v}}^\rho\right)\right],\end{aligned}$$

[3] For explicit expressions and more details on Φ_B and Φ_V, see [22, 25] and references therein.

[4] For more details of various contributions and the corresponding Feynman loops, see for example [26] and references therein.

$$a^c_{\rm ann}(\rho^0\gamma) = Q_d\left[a_4 b^\rho + a_6\left(d^\rho_v + d^\rho_{\bar v}\right)\right],$$
$$a^c_{\rm ann}(\rho^-\gamma) = Q_u\left[a_4 b^\rho + a_6\left(-2d^\rho_v + d^\rho_{\bar v}\right)\right] \quad (34)$$

for $\overline{B} \to \rho\gamma$ decays, where $Q_u = 2/3$ and $Q_d = -1/3$ are the electric charge of up and down quarks, and a_i denote the combinations of LO Wilson coefficients

$$a_{1,2} = C^0_{1,2} + \frac{1}{3}C^0_{2,1},$$
$$a_4 = C^0_4 + \frac{1}{3}C^0_3,$$
$$a_6 = C^0_6 + \frac{1}{3}C^0_5\,. \quad (35)$$

And finally the functions b^V, d^V_v and $d^V_{\bar v}$ are [26]

$$b^V = \frac{2\pi^2}{F_V}\frac{f_B m_V f_V}{m_B m_b \lambda_B}\,, \quad (36)$$

$$d^V_{\substack{(-)\\ v}} = -\frac{4\pi^2}{F_V}\frac{f_B f^\perp_V}{m_B m_b}\left(1 \mp \alpha^V_1 + \alpha^V_2 + \ldots\right). \quad (37)$$

The values of all parameters appearing in the above two equations can be found in Table 3.

One special feature of the $B \to \rho\gamma$ decay is that the weak annihilation can proceed through the current–current operator with large Wilson coefficient C_1. Although the annihilation contribution is power-suppressed in $1/m_b$, this is compensated for by the large Wilson coefficient and the occurrence of annihilation at tree level.

From the decay amplitude in (30), it is straightforward to write down the branching ratio for $\overline{B} \to V\gamma$ decay:

$$\mathcal{B}(\overline{B} \to V\gamma) = \tau_B \frac{G^2_{\rm F}\alpha m^3_B m^2_b}{32\pi^4}\left(1 - \frac{m^2_V}{m^2_B}\right)^3 |R_V|^2\, c^2_V |F_V|^2, \quad (38)$$

where the function R_V has been given in (31), and $c_V = 1$ for $V = K^*, \rho^-$ and $c_V = 1/\sqrt{2}$ for $V = \rho^0$. The branching ratios for the CP-conjugated $B \to V\gamma$ decay are obtained by the replacement of $\lambda^{(q)}_p \to \lambda^{(q)*}_p$ in function R_V.

2.3 Outline of the general 2HDM's

The simplest extension of the SM is the so-called two-Higgs-doublet models [12]. In such models, the tree level flavor changing neutral currents are absent if one introduces an ad hoc discrete symmetry to constrain the 2HDM scalar potential and Yukawa Lagrangian. Let us consider a Yukawa Lagrangian of the form [34]

$$\mathcal{L}_Y = \eta^U_{ij}\bar{Q}_{i,\rm L}\tilde{\phi}_1 U_{j,\rm R} + \eta^D_{ij}\bar{Q}_{i,\rm L}\phi_1 D_{j,\rm R} + \xi^U_{ij}\bar{Q}_{i,\rm L}\tilde{\phi}_2 U_{j,\rm R} + \xi^D_{ij}\bar{Q}_{i,\rm L}\phi_2 D_{j,\rm R} + \text{H.c.}\,, \quad (39)$$

where ϕ_i $(i = 1, 2)$ are the two Higgs doublets, $\tilde{\phi}_{1,2} = {\rm i}\tau_2\phi^*_{1,2}$, $Q_{i,\rm L}$ ($U_{j,\rm R}$) with $i = (1, 2, 3)$ are the left-handed isodoublet quarks (right-handed up-type quarks), $D_{j,\rm R}$ are the right-handed isosinglet down-type quarks, while $\eta^{U,D}_{i,j}$ and $\xi^{U,D}_{i,j}$ ($i, j = 1, 2, 3$ are family indices) are generally the non-diagonal matrices of the Yukawa coupling. By imposing the discrete symmetry

$$\phi_1 \to -\phi_1,\ \phi_2 \to \phi_2,\ D_i \to -D_i,\ U_i \to \mp U_i\,, \quad (40)$$

one obtains the so-called model I and model II.

In model III [34,35], the third type of two-Higgs-doublet models, no discrete symmetry is imposed and both up- and down-type quarks may have diagonal and/or flavor changing couplings with ϕ_1 and ϕ_2. As described in [34], one can choose a suitable basis to express the two Higgs doublet ϕ_1 and ϕ_2 and define the mass eigenstates $(H^\pm, \overline{H}^0, h^0, A^0)$. After the rotation of quark fields, the Yukawa Lagrangian of the quarks are of the form [34]

$$\mathcal{L}^{\rm III}_Y = \eta^U_{ij}\bar{Q}_{i,\rm L}\tilde{\phi}_1 U_{j,\rm R} + \eta^D_{ij}\bar{Q}_{i,\rm L}\phi_1 D_{j,\rm R} + \hat{\xi}^U_{ij}\bar{Q}_{i,\rm L}\tilde{\phi}_2 U_{j,\rm R} + \hat{\xi}^D_{ij}\bar{Q}_{i,\rm L}\phi_2 D_{j,\rm R} + \text{H.c.}\,, \quad (41)$$

where $\eta^{U,D}_{ij}$ correspond to the diagonal mass matrices of up- and down-type quarks, while the neutral and charged flavor changing couplings will be [34]

$$\hat{\xi}^{U,D}_{\rm neutral} = \xi^{U,D}, \qquad \hat{\xi}^U_{\rm charged} = \xi^U V_{\rm CKM},$$
$$\hat{\xi}^D_{\rm charged} = V_{\rm CKM}\xi^D\,, \quad (42)$$

with

$$\xi^{U,D}_{ij} = \frac{g\sqrt{m_i m_j}}{\sqrt{2}M_W}\lambda_{ij}\,, \quad (43)$$

where $V_{\rm CKM}$ is the CKM mixing matrix [29], and $i, j = (1, 2, 3)$ are the generation indices. The coupling constants λ_{ij} are free parameters to be determined by experiment, and they may also be complex.

The two-Higgs-doublet models have been studied extensively in the literature at LO and NLO level [8,13,34–43] and tested experimentally [31]. For model I, the new physics corrections to physical observables are usually very small and less interesting phenomenologically. Model II, however, has been very popular, since it is the building block of the minimal supersymmetric standard model and may provide large contributions to the mixing and decay processes of the K and B meson systems. The most stringent constraint on model II may come from the inclusive $B \to X_s\gamma$ decay. From the experimental measurements and currently available studies at NLO level [8, 13, 37–39], one gets to know the following main features of the conventional models I and II, and model III.

(1) For model I, no bound on M_H can be obtained from $B \to X_s\gamma$ [44], since the charged Higgs loops interfere destructively with the SM penguin diagrams and decouple for large $\tan\beta$.

(2) In model II, the charged Higgs penguins interfere constructively with their SM counterparts, and thus always enhance the branching ratio $\mathcal{B}(B \to X_s\gamma)$. The measured mass splitting $\Delta M_{B_d} = 0.502 \pm 0.007\,{\rm ps}^{-1}$ and the decay rate $\mathcal{B}(B \to X_s\gamma) = (3.34 \pm 0.38) \times 10^{-4}$ leads to strong bounds on both the $\tan\beta = v_2/v_1$ and the mass

M_H [13,44]. The typical bounds at NLO level as given for example in [13] are

$$\tan\beta > 0.6 \tag{44}$$

and

$$M_H \gtrsim 300\,\text{GeV} \tag{45}$$

for any value of $\tan\beta$, and the $\tan\beta$ dependence of the lower bound saturates for $\tan\beta \gtrsim 5$. This NLO lower bound on M_H is much stronger than the direct experimental bound $M_H > 78.6\,\text{GeV}$ [31] and the bound from other observables, such as R_b and $B \to \tau$ decays [8].

(3) For model III[5], the charged-Higgs loop diagrams can provide significant contributions to B^0–$\overline{B}^0$ mixing, the inclusive $B \to X_s\gamma$ decay and many other physical observables [34,41]. In a previous paper [13], we calculated the charged-Higgs contributions to the mass splitting ΔM_{B_d} and the decay rate $\mathcal{B}(B \to X_s\gamma)$ at the NLO level, and found the strong constraints on free parameters λ_{tt}, λ_{bb} and M_H from the well measured ΔM_{B_d} and $\mathcal{B}(B \to X_s\gamma)$. Two typical choices of $(\lambda_{tt}, \lambda_{bb})$ and the corresponding constraint on M_H obtained from the measured branching ratio of $B \to X_s\gamma$ decay are

$$\text{III}-\text{A}: (\lambda_{tt}, \lambda_{bb}) = (0.5, 1), \quad M_H > 150\,\text{GeV} \tag{46}$$

as shown in Fig. 9 of [13]; and

$$\text{III}-\text{B}: (\lambda_{tt}, \lambda_{bb}) = (0.5, 22), \quad 226 \le M_H \le 285\,\text{GeV}. \tag{47}$$

For the first case, the new physics contribution to $B \to X_s\gamma$ is very small and becomes negligible for $M_H > 250\,\text{GeV}$. For the second case (in [13], it was denoted case C), the new physics contribution can be rather large, the sign of the dominant Wilson coefficient $C_7^{\text{eff}}(m_b)$ changed its sign from negative to positive due to the inclusion of the charged-Higgs penguin contributions. In this paper, we denote these two typical cases as model III-A and III-B, respectively.

2.4 NLO Wilson coefficients in the general 2HDM's

The new physics contributions to the quark level $b \to s/d\gamma$ transition from the charged Higgs penguins manifest themselves from the correction to the Wilson coefficients at the matching scale M_W. In [37], the authors calculated the NLO QCD corrections to the $B \to X_s\gamma$ decay in the conventional models I and II. In [13], we extended their work to the case of model III. Here we firstly present the Wilson coefficients at the energy scales M_W and $\mu = \mathcal{O}(m_b)$ in a general 2HDM and then calculate the branching ratios, CP and isospin asymmetries, and the U-spin symmetry breaking of the exclusive decays $B \to K^*\gamma$ and $B \to \rho\gamma$ in the following sections.

Note that the CMM basis was used in [13,37]; the Wilson coefficients $C_i^{\text{eff}}(\mu)$ there are indeed the Wilson coefficients $Z_i(\mu)$ in this paper. For the exclusive decays $B \to V\gamma$ and to the first order in α_s, only the NLO expression for $C_7(\mu)$ has to be used while the leading order values are sufficient for the other Wilson coefficients appearing in $a_7^p(V\gamma)$ in (32). Therefore, only $C_7(\mu)$, $C_8^{(0)}(\mu)$ and $Z_8^{(0)}(\mu)$ in (32) are affected by the charged-Higgs penguin contributions, while all other Wilson coefficients for $i = 1, \ldots, 6$ remain the same as in the SM. Since $Z_{7,8}^0(\mu) = C_{7,8}^0(\mu)$, and $C_7^1(\mu) = Z_7^1(\mu)$ [26], so we here use the terms $C_{7,8}^0$ and C_7^1 for convenience.

The new physics part of the LO Wilson coefficients $C_{7,8}^0$ at the matching energy scale M_W takes the form

$$C_{7,\text{NP}}^0(M_W) = -\frac{1}{6}|Y|^2 A(y_t) + (XY^*)B(y_t)\,, \tag{48}$$

$$C_{8,\text{NP}}^0(M_W) = -\frac{1}{6}|Y|^2 D(y_t) + (XY^*)E(y_t)\,, \tag{49}$$

where $y_t = m_t^2/M_H^2$, and the functions $A(x)$ and $D(x)$ have been given in (10) and (11), while

$$B(y) = \frac{3y - 5y^2}{12(1-y)^2} + \frac{2y - 3y^2}{6(1-y)^3}\log[y]\,, \tag{50}$$

$$E(y) = \frac{3y - y^2}{4(1-y)^2} + \frac{y}{2(1-y)^3}\log[y]\,. \tag{51}$$

The new physics parts of the NLO Wilson coefficients $C_{7,8}^1$ at the matching scale μ_W can be written as

$$C_{7,\text{NP}}^1(M_W) = |Y|^2\, C_{7,YY}^1(M_W) + (XY^*)\, C_{7,XY}^1(M_W), \tag{52}$$

$$C_{8,\text{NP}}^1(M_W) = |Y|^2\, C_{8,YY}^1(M_W) + (XY^*)\, C_{8,XY}^1(M_W)\,, \tag{53}$$

with

$$C_{i,YY}^1(M_W) = W_{i,YY} + M_{i,YY}\ln[y_t] + T_{i,YY}\left(\ln[x_t] - \frac{4}{3}\right), \tag{54}$$

$$C_{i,XY}^1(M_W) = W_{i,XY} + M_{i,XY}\ln[y_t] + T_{i,XY}\left(\ln[x_t] - \frac{4}{3}\right). \tag{55}$$

The explicit expressions of the functions $W_{i,j}$, $M_{i,j}$ and $T_{i,j}$ ($i = 7, 8$ and $j = YY, XY$) can be found in [37] or in Appendix B. The T_{ij} terms appear when expressing $\overline{m}_t(M_W)$ in terms of the pole mass m_t in the corresponding lowest order coefficients [37].

At the low energy scale $\mu = \mathcal{O}(m_b)$, the Wilson coefficients $C_7^{0,1}(\mu)$ and $C_8^0(\mu)$ after the inclusion of new physics contributions can be written as

$$C_7^0(\mu) = \eta^{\frac{16}{23}}\left[C_{7,\text{SM}}^0(M_W) + C_{7,\text{NP}}^0(M_W)\right]$$

[5] In this paper, the term model III always means the scenario of the general model III as presented in [41]. In such a model III [41], only the couplings λ_{tt} and λ_{bb} remain non-zero, and only the charged Higgs boson penguin diagram provide a new physics contribution to $b \to s\gamma$ decay at one loop level. For more details see [13,41].

$$+\frac{8}{3}\left(\eta^{\frac{14}{23}}-\eta^{\frac{16}{23}}\right)\left[C^0_{8,\rm SM}(M_W)+C^0_{8,\rm NP}(M_W)\right] +\sum_{i=1}^{8} h_i\,\eta^{a_i}\,, \tag{56}$$

$$C^0_8(\mu)=\eta^{\frac{14}{23}}\left[C^0_{8,\rm SM}(M_W)+C^0_{8,\rm NP}(M_W)\right]+\sum_{i=1}^{8}\hbar_i\,\eta^{a_i}\,, \tag{57}$$

$$\begin{aligned} C^1_7(\mu_b) &= \eta^{\frac{39}{23}}\left[C^1_{7,\rm SM}(M_W)+C^1_{7,\rm NP}(M_W)\right] \\ &+\frac{8}{3}\left(\eta^{\frac{37}{23}}-\eta^{\frac{39}{23}}\right)\left[C^1_{8,\rm SM}(M_W)+C^1_{8,\rm NP}(M_W)\right] \\ &+\left(\frac{297664}{14283}\eta^{\frac{16}{23}}-\frac{7164416}{357075}\eta^{\frac{14}{23}}+\frac{256868}{14283}\eta^{\frac{37}{23}}\right. \\ &\quad\left.-\frac{6698884}{357075}\eta^{\frac{39}{23}}\right)\left[C^0_{8,\rm SM}(M_W)+C^0_{8,\rm NP}(M_W)\right] \\ &+\frac{37208}{4761}\left(\eta^{\frac{39}{23}}-\eta^{\frac{16}{23}}\right)\left[C^0_{7,\rm SM}(M_W)+C^0_{7,\rm NP}(M_W)\right] \\ &+\sum_{i=1}^{8}\left[e_i\eta E(x_t)+f_i+g_i\eta)\eta^{a_i}\right]\eta^{a_i}\,, \end{aligned} \tag{58}$$

where the "magic numbers" are listed in Table 2.

In the conventional model I and II, the general Yukawa couplings X and Y are real and given by

$$X=-\cot\beta,\quad Y=\cot\beta\quad(\text{model}\quad \text{I})\,, \tag{59}$$

$$X=\tan\beta,\quad Y=\cot\beta\quad(\text{model}\quad \text{II})\,. \tag{60}$$

In model III where only the couplings λ_{tt} and λ_{bb} are non-zero, the relation between the couplings (X, Y) and $(\lambda_{tt}, \lambda_{bb})$ is also simple:

$$X=-\lambda_{bb},\quad Y=\lambda_{tt}\quad(\text{model}\quad \text{III})\,. \tag{61}$$

Now we are ready to calculate the numerical results for the $B \to V\gamma$ decay in the general 2HDM's with the inclusion of NLO QCD corrections.

3 $B \to K^*\gamma$ decay

For the numerical calculations, unless otherwise specified, we use the central values of the input parameters as listed in Table 3 and consider the uncertainties of those parameters as given explicitly in Table 3.

From (30) and (38), the decay amplitude and branching ratio for $B \to K^*\gamma$ decay can be written as

$$A(\overline{B}\to K^*\gamma)=\frac{G_{\rm F}}{\sqrt{2}}R_{K^*}\langle K^*\gamma|Q_7|\overline{B}\rangle\,, \tag{62}$$

$$\mathcal{B}(\overline{B}\to K^*\gamma)= \tau_B\frac{G^2_{\rm F}\alpha m^3_B m^2_b}{32\pi^4}\left(1-\frac{m^2_{K^*}}{m^2_B}\right)^3|R_{K^*}|^2\,|F^*_K|^2, \tag{63}$$

with

$$\begin{aligned} R_{K^*} &= V^*_{us}V_{ub}\,\left[a^u_7(K^*\gamma)+a^u_{\rm ann}(K^*\gamma)\right] \\ &+V^*_{cs}V_{cb}\,\left[a^c_7(K^*\gamma)+a^c_{\rm ann}(K^*\gamma)\right]\,. \end{aligned} \tag{64}$$

The CP asymmetry of $B \to K^*\gamma$ can also be defined as [15,16]

$$\mathcal{A}_{CP}(K^*\gamma)=\frac{\Gamma(B\to K^*\gamma)-\Gamma(\overline{B}\to\overline{K}^*\gamma)}{\Gamma(B\to K^*\gamma)+\Gamma(\overline{B}\to\overline{K}^*\gamma)}\,. \tag{65}$$

Another physical observable for $B \to V\gamma$ decay is the isospin symmetry breaking in the $K^{*\pm}$–$\overline{K}^{*0}$ or $\rho^{\pm}$–ρ^0 system. Since the branching ratios of both $B^- \to K^{*-}\gamma$ and $\overline{B}^0 \to \overline{K}^{*0}\gamma$ decays have been measured, the study of the isospin breaking in $B \to V\gamma$ decays becomes very interesting now [27,28]. Following [27], the breaking of isospin symmetry in the K^{*-}–$\overline{K}^{*0}$ system can be defined as

$$\Delta_{0-}(K^*\gamma)\equiv\frac{\eta_\tau\mathcal{B}(B\to\overline{K}^{*0}\gamma)-\mathcal{B}(B\to K^{*-}\gamma)}{\eta_\tau\mathcal{B}(B\to\overline{K}^{*0}\gamma)+\mathcal{B}(B\to K^{*-}\gamma)}\,, \tag{66}$$

where $\eta_\tau=\tau_{B^+}/\tau_{B^0}$, and the CP-averaged branching ratios are understood.

By using the world averages as given in (2) and the ratio $\tau_{B^+}/\tau_{B^0}=1.083\pm0.017$ [31], we find numerically that

$$\Delta_{0-}(K^*\gamma)^{\rm exp}=(3.9\pm4.8)\%\,, \tag{67}$$

where the errors from the two measured branching ratios and the ratio τ_{B^+}/τ_{B^0} have been added in quadrature. The measured value of isospin symmetry breaking is indeed small as expected previously [15,16]. Any new physics contribution producing large isospin breaking for $B \to K^*\gamma$ decays will be strongly constrained by this measurement.

3.1 Branching ratios and CP asymmetries

By using the formulas as given in (32) and (33) and the central values of input parameters in Table 3, we find the SM predictions for $a^p_7(K^*\gamma)$ and $a_{\rm ann}(K^*\gamma)$ at the low energy scale $\mu = m_b$,

$$\begin{aligned} &a^u_7(K^*\gamma) \\ &=\underbrace{-0.3212}_{C^0_{7,\rm SM}(m_b)}+\underbrace{0.0113}_{\Delta C^1_{7,\rm SM}}\underbrace{-0.1407-0.0683{\rm i}}_{T^{\rm I}-\rm contribution} \\ &\quad\underbrace{+0.0330-0.0002{\rm i}}_{T^{\rm II}-\rm contribution} \\ &=-0.4177-0.0685{\rm i}\,, \\ &a^c_7(K^*\gamma) \\ &=\underbrace{-0.3212}_{C^0_{7,\rm SM}(m_b)}+\underbrace{0.0113}_{\Delta C^1_{7,\rm SM}}\underbrace{-0.0802-0.0131{\rm i}}_{T^{\rm I}-\rm contribution} \\ &\quad\underbrace{-0.0161-0.0120{\rm i}}_{T^{\rm II}-\rm contribution} \end{aligned} \tag{68}$$

$$= -0.4063 - 0.0251\mathrm{i}\,, \tag{69}$$

$$a^u_{\rm ann}(\overline{K}^{*0}\gamma) = a^c_{\rm ann}(\overline{K}^{*0}\gamma) = -0.0092, \tag{70}$$

$$a^u_{\rm ann}(K^{*-}\gamma) = 0.1933, \tag{71}$$

$$a^c_{\rm ann}(K^{*-}\gamma) = 0.0046. \tag{72}$$

It is easy to see that
(a) the type-I contribution is about 4 times larger than the type-II contribution, and
(b) only the weak annihilation factor $a^u_{\rm ann}(K^{*-}\gamma)$ contributes to the decay $B \to K^*\gamma$ effectively, since for the $b \to u$ transition the power suppression is compensated for by the large Wilson coefficient C_1 and the occurrence of annihilation at tree level.

The corresponding NLO SM predictions for branching ratio $\mathcal{B}(B \to K^*\gamma)$ are

$$\begin{aligned}&\mathcal{B}(B \to \overline{K}^{*0}\gamma)^{\rm SM}\\ &= \left[3.35^{+1.62}_{-1.30}(F_{K^*})^{+0.57}_{-0.60}(\mu)^{+0.27}_{-0.10}(\lambda_B) \pm 0.20(m_c)\right] \times 10^{-5}\\ &= \left(3.35^{+1.75}_{-1.45}\right) \times 10^{-5}\,,\end{aligned} \tag{73}$$

$$\begin{aligned}&\mathcal{B}(B \to K^{*-}\gamma)^{\rm SM}\\ &= \left[3.25^{+1.67}_{-1.33}(F_{K^*})^{+0.25}_{-0.47}(\mu)^{+0.35}_{-0.14}(\lambda_B) \pm 0.20(m_c)\right] \times 10^{-5}\\ &= \left(3.25^{+1.74}_{-1.43}\right) \times 10^{-5}\,,\end{aligned} \tag{74}$$

where the four major errors have been added in quadrature. The uncertainty of the form factor F_{K^*} dominate the theoretical error, and the remaining errors from other input parameters are negligibly small. Although the central values of the SM predictions for the decay rates are smaller than the world average as given in (2), they are in good agreement within 1σ theoretical error. The effect of the annihilation contribution on the decay rates is less than 5% numerically.

If we use $F_{K^*} = 0.38 \pm 0.06$ as obtained from the light-cone sum rule (LCSR) [32] instead of $F_{K^*} = 0.25 \pm 0.06$ in our numerical calculation, we find

$$\mathcal{B}(B \to \overline{K}^{*0}\gamma)^{\rm SM} = \left(7.27^{+2.58}_{-2.37}\right) \times 10^{-5}\,, \tag{75}$$

$$\mathcal{B}(B \to K^{*-}\gamma)^{\rm SM} = \left(7.31^{+2.57}_{-2.37}\right) \times 10^{-5}\,. \tag{76}$$

Here the central values are much larger than the measured values as given in (2), but still agree with the data within 2σ errors because of the large theoretical error. For the purpose of studying the new physics contributions to the exclusive decays $B \to V\gamma$, one prefers a better agreement between the SM predictions and the high precision data. Therefore, we will use $F_{K^*} = 0.25 \pm 0.06$ in this paper, unless otherwise specified.

For model I, the theoretical predictions for the branching ratios are

$$\mathcal{B}(B \to \overline{K}^{*0}\gamma)^I = \left(3.35^{+1.75}_{-1.45}\right) \times 10^{-5}\,, \tag{77}$$

$$\mathcal{B}(B \to K^{*-}\gamma)^I = \left(3.25^{+1.74}_{-1.43}\right) \times 10^{-5}\,, \tag{78}$$

for $\tan\beta = 4$ and $M_H = 200\,\mathrm{GeV}$. The M_H dependence of the branching ratio $\mathcal{B}(B \to K^*\gamma)$ is very weak: it will change by less than 2% in the range of $200 \le M_H \le 600\,\mathrm{GeV}$.

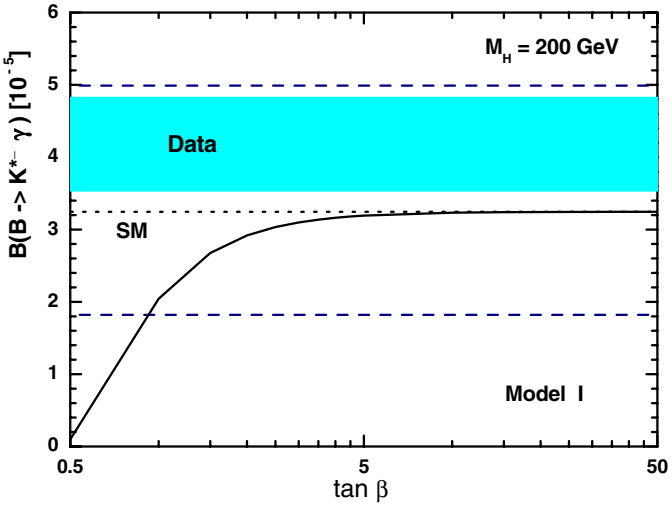

Fig. 1. Plot of the branching ratio $\mathcal{B}(B \to K^{*-}\gamma)$ versus $\tan\beta$ in model I for $M_H = 200\,\mathrm{GeV}$. The dots and solid line show the central value of the SM and model I prediction, respectively. The region between the two dashed lines shows the SM prediction: $\mathcal{B}(B \to K^{*-}\gamma) = (3.25^{+1.74}_{-1.43}) \times 10^{-5}$. The shaded band shows the data within 2σ errors: $\mathcal{B}(B \to K^{*-}\gamma)^{\rm exp} = (4.18 \pm 0.64) \times 10^{-5}$

Figure 1 shows the $\tan\beta$ dependence of the branching ratio $\mathcal{B}(B \to K^{*-}\gamma)$ in model I for $M_H = 200\,\mathrm{GeV}$. The dots and solid line show the central value of the NLO SM and model I prediction, respectively. The region between the two dashed lines shows the NLO SM prediction with error as given in (74). The shaded band shows the data: $\mathcal{B}(B \to K^{*-}\gamma)^{\rm exp} = (4.18 \pm 0.32) \times 10^{-5}$. From this figure, one can see that (a) the NLO SM prediction agree with the data within 1σ error; and (b) the new physics contribution in model I is negligibly small for $\tan\beta \ge 1$, while $\tan\beta < 0.5$ is also strongly disfavored. For the $B \to K^{*0}\gamma$ decay mode, we have the same conclusion.

In the popular model II, the numerical results for $a^p_7(K^*\gamma)$ at the low energy scale $\mu = m_b$ are,

$$\begin{aligned}a^u_7(K^*\gamma)^{\rm II} &= \underbrace{-0.3100}_{C_{7,\rm SM}(m_b)} - \underbrace{0.06523}_{\Delta C_{7,\rm NP}} \underbrace{-0.1436 - 0.0724\mathrm{i}}_{T^{\rm I}-\rm contribution}\\ &\quad \underbrace{+0.0481 - 0.0003\mathrm{i}}_{T^{\rm II}-\rm contribution}\\ &= -0.4707 - 0.0728\mathrm{i}\,,\end{aligned} \tag{79}$$

$$\begin{aligned}a^c_7(K^*\gamma)^{\rm II} &= \underbrace{-0.3100}_{C_{7,\rm SM}(m_b)} - \underbrace{0.0652}_{\Delta C_{7,\rm NP}} \underbrace{-0.0831 - 0.0172\mathrm{i}}_{T^{\rm I}-\rm contribution}\\ &\quad \underbrace{-0.0265 - 0.0182\mathrm{i}}_{T^{\rm II}-\rm contribution}\\ &= -0.4848 - 0.0354\mathrm{i}\,,\end{aligned} \tag{80}$$

for $\tan\beta = 4$ and $M_H = 300\,\mathrm{GeV}$. The second terms in above two equations are the new physics corrections to the NLO Wilson coefficient $C_{7,\rm SM}(m_b)$, the hard vertex

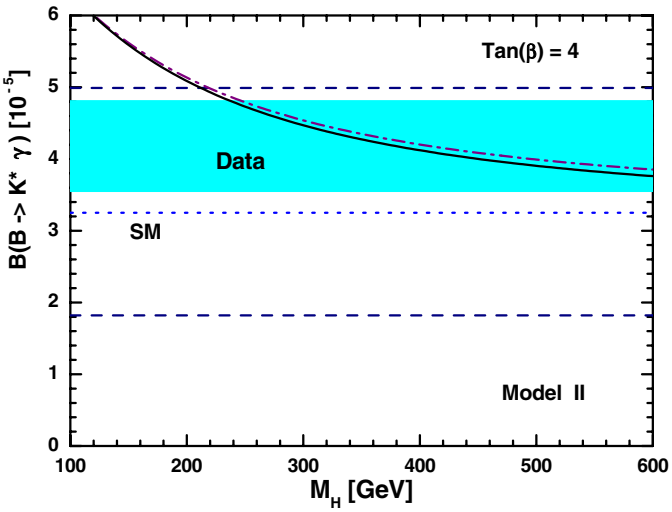

Fig. 2. The M_H dependence of the branching ratio $\mathcal{B}(B \to K^*\gamma)$ in model II for $\tan\beta = 4$. The dot-dashed and solid curve show the central value of the NLO model II prediction for $\mathcal{B}(B \to K^{*0}\gamma)$ and $\mathcal{B}(B \to K^{*-}\gamma)$, respectively. The region between two dashed lines shows the SM prediction: $\mathcal{B}(B \to K^{*-}\gamma) = (3.25^{+1.74}_{-1.43}) \times 10^{-5}$. The shaded band shows the same data as in Fig. 1

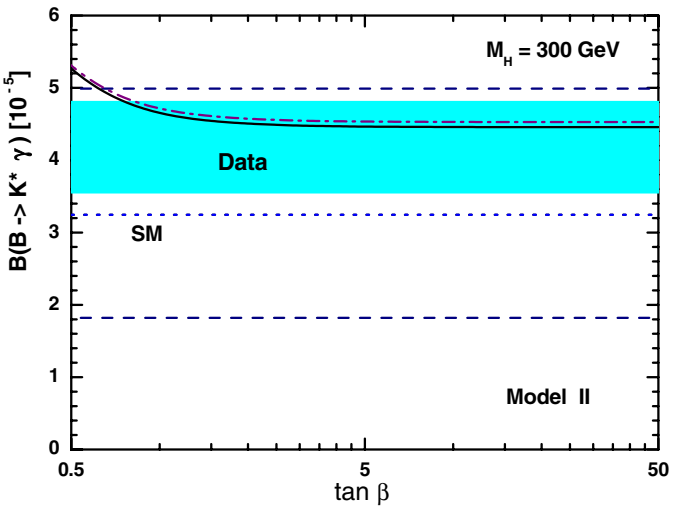

Fig. 3. The $\tan\beta$ dependence of the branching ratio $\mathcal{B}(B \to K^*\gamma)$ in model II for $M_H = 300\,\text{GeV}$. The curves and bands have the same meaning as in Fig. 2

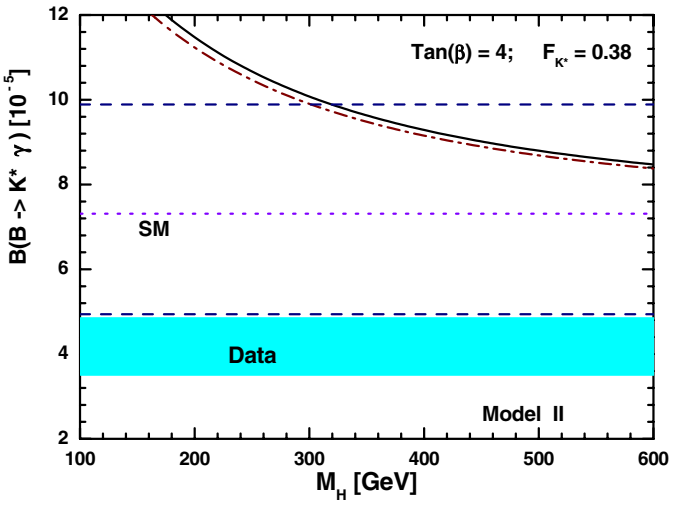

Fig. 4. The same as Fig. 2, but for $F_{K^*} = 0.38 \pm 0.06$ instead of $F_{K^*} = 0.25 \pm 0.06$

and hard spectator contributions are also changed slightly because of the variations of $Z_8^0(\mu)$ and $C_7^0(\mu_h)$ after including the charged-Higgs contributions. The total new physics contribution to a_7^p in model II is around 10% for $\tan\beta = 4$ and $M_H = 300\,\text{GeV}$. The annihilation parts remain unchanged.

For model II, the theoretical predictions for branching ratios are

$$\begin{aligned}
&\mathcal{B}(B \to \overline{K}^{*0}\gamma)^{\text{II}} \\
&= \left[4.54^{+2.22}_{-1.77}(F_{K^*})^{+0.68}_{-0.72}(\mu)^{+0.33}_{-0.13}(\lambda_B) \pm 0.22(m_c)\right] \\
&\qquad \times 10^{-5} \\
&= \left(4.54^{+2.36}_{-1.93}\right) \times 10^{-5}\,, \qquad (81) \\
&\mathcal{B}(B \to K^{*-}\gamma)^{\text{II}} \\
&= \left[4.47^{+2.29}_{-1.83}(F_{K^*})^{+0.32}_{-0.57})(\mu)^{+0.44}_{-0.17}(\lambda_B) \pm 0.23(m_c)\right] \\
&\qquad \times 10^{-5} \\
&= \left(4.47^{+2.36}_{-1.94}\right) \times 10^{-5}\,, \qquad (82)
\end{aligned}$$

for $\tan\beta = 4$ and $M_H = 300\,\text{GeV}$.

Figure 2 shows the M_H dependence of the branching ratio $B \to K^*\gamma$ in model II for $\tan\beta = 4$. The dot-dashed and solid curve shows the central value of the NLO model II prediction for the branching ratio $\mathcal{B}(B \to \overline{K}^{*0}\gamma)$ and $\mathcal{B}(B \to K^{*-}\gamma)$, respectively. Other bands or lines show the same thing as in Fig. 1.

Figure 3 shows the $\tan\beta$ dependence of the branching ratio $B \to K^*\gamma$ in model II for $M_H = 300\,\text{GeV}$. The dot-dashed and solid curve shows the central value of the NLO model II prediction for the branching ratio $\mathcal{B}(B \to \overline{K}^{*0}\gamma)$ and $\mathcal{B}(B \to K^{*-}\gamma)$, respectively. Other bands or lines show the same thing as in Fig. 1.

It is easy to see from Fig. 2 that a charged Higgs boson with a mass around 200 GeV is still allowed by the measured branching ratio of the exclusive $B \to K^*\gamma$ decay, which is weaker than the lower bound of $M_H \gtrsim 300\,\text{GeV}$ obtained from the data of the inclusive $B \to X_s\gamma$ decay. This is consistent with general expectations. The key point here is the large uncertainty of the non-perturbative form factor F_{K^*}. If we use $F_{K^*} = 0.38 \pm 0.06$ and keep all other input parameters unchanged, we get a much stronger lower limit on M_H, as can be seen from Fig.4, where the solid and dot-dashed curves show the NLO model II prediction for $\mathcal{B}(B \to \overline{K}^{*0}\gamma)$ and $\mathcal{B}(B \to K^{*-}\gamma)$, respectively. The dots line and the band between two dashed lines show the corresponding SM prediction of $\mathcal{B}(B \to K^{*-}\gamma) = (7.31^{+2.58}_{-2.37})$ for $F_{K^*} = 0.38 \pm 0.06$.

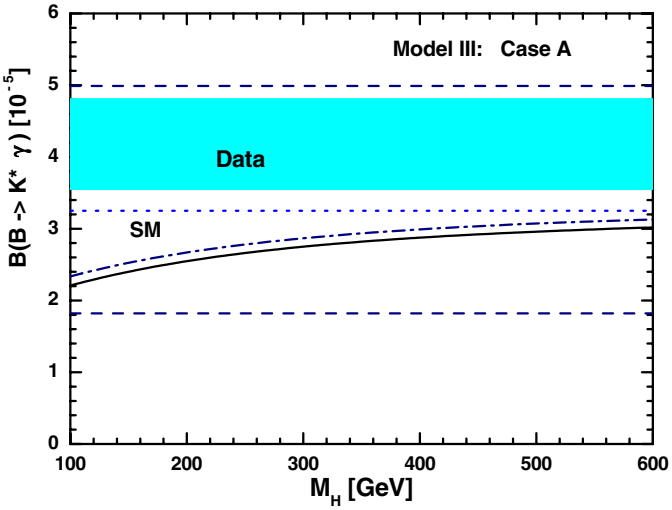

Fig. 5. The M_H dependence of the branching ratio $\mathcal{B}(B \to K^*\gamma)$ in model III-A. The dot-dashed and solid curve show the central value of the NLO model III-A prediction for $\mathcal{B}(B \to \overline{K}^{*0}\gamma)$ and $\mathcal{B}(B \to K^{*-}\gamma)$, respectively. The region between the two dashed lines shows the SM prediction: $\mathcal{B}(B \to K^{*-}\gamma) = (3.25^{+1.74}_{-1.43}) \times 10^{-5}$. The shaded band shows the measured $\mathcal{B}(B \to K^{*-}\gamma)$ within 2σ errors

Now we study model III. According to previous studies in [13], we got to know that the charged Higgs penguins can provide a significant contribution to the dominant Wilson coefficient $C_7(\mu)$ and changed its sign from negative to positive. Of course, the size of the new physics contributions is strongly constrained by the measured branching ratio of the inclusive $B \to X_s\gamma$, as investigated in detail in [13].

For model III-A, i.e. $(\lambda_{tt}, \lambda_{bb}) = (0.5, 1)$, the new physics contributions are small, the numerical results for $a_7^p(K^*\gamma)$ at the low energy scale $\mu = m_b$ are

$$\begin{aligned} a_7^u(K^*\gamma)^{\mathrm{III-A}} &= \underbrace{-0.3100}_{C_{7,\mathrm{SM}}(m_b)} + \underbrace{0.0299}_{\Delta C_{7,\mathrm{NP}}} \underbrace{-0.1394 - 0.0664\mathrm{i}}_{T^{\mathrm{I}}-\mathrm{contribution}} \\ &\quad \underbrace{+0.0336 - 0.0002\mathrm{i}}_{T^{\mathrm{II}}-\mathrm{contribution}} \\ &= -0.3859 - 0.0666\mathrm{i}\,, \qquad (83) \\ a_7^c(K^*\gamma)^{\mathrm{III-A}} &= \underbrace{-0.3100}_{C_{7,\mathrm{SM}}(m_b)} + \underbrace{0.0299}_{\Delta C_{7,\mathrm{NP}}} \underbrace{-0.0788 - 0.0112\mathrm{i}}_{T^{\mathrm{I}}-\mathrm{contribution}} \\ &\quad \underbrace{-0.0155 - 0.0120\mathrm{i}}_{T^{\mathrm{II}}-\mathrm{contribution}} \\ &= -0.3744 - 0.0231\mathrm{i}\,, \qquad (84) \end{aligned}$$

for $M_H = 300\,\mathrm{GeV}$. The total new physics contribution to a_7^p in model III-A is also around 10% in magnitude for $M_H = 300\,\mathrm{GeV}$, but in the opposite direction of that in model II. The annihilation parts also remain unchanged.

Figure 5 shows the M_H dependence of the branching ratio $B \to K^*\gamma$ in model III-A. The dot-dashed and solid curve shows the central value of the NLO model III prediction for the branching ratio $\mathcal{B}(B \to \overline{K}^{*0}\gamma)$ and $\mathcal{B}(B \to K^{*-}\gamma)$, respectively. Other bands or lines show the same thing as in Fig. 1. The new physics contribution here is small but consistent with the SM prediction within 1σ error. Numerically, we have

$$\mathcal{B}(B \to \overline{K}^{*0}\gamma)^{\mathrm{III-A}} = \left(2.87^{+1.50}_{-1.27}\right) \times 10^{-5}\,, \qquad (85)$$

$$\mathcal{B}(B \to K^{*-}\gamma)^{\mathrm{III-A}} = \left(2.75^{+1.48}_{-1.22}\right) \times 10^{-5}\,, \qquad (86)$$

for $M_H = 300\,\mathrm{GeV}$, where the four major errors as in (81) and (82) have been added in quadrature.

For model III-B, i.e. $(\lambda_{tt}, \lambda_{bb}) = (0.5, 22)$, the new physics contributions are large; the numerical results for $a_7^p(K^*\gamma)$ at the low energy scale $\mu = m_b$ are

$$\begin{aligned} a_7^u(K^*\gamma)^{\mathrm{III-B}} &= \underbrace{-0.3100}_{C_{7,\mathrm{SM}}(m_b)} + \underbrace{0.8485}_{\Delta C_{7,\mathrm{NP}}} \underbrace{-0.1049 - 0.0174\mathrm{i}}_{T^{\mathrm{I}}-\mathrm{contribution}} \\ &\quad \underbrace{+0.0752 - 0.0003\mathrm{i}}_{T^{\mathrm{II}}-\mathrm{contribution}} \\ &= 0.5088 - 0.0177\mathrm{i}\,, \qquad (87) \\ a_7^c(K^*\gamma)^{\mathrm{III-B}} &= \underbrace{-0.3100}_{C_{7,\mathrm{SM}}(m_b)} + \underbrace{0.8485}_{\Delta C_{7,\mathrm{NP}}} \underbrace{-0.0443 + 0.0379\mathrm{i}}_{T^{\mathrm{I}}-\mathrm{contribution}} \\ &\quad \underbrace{+0.0005 - 0.0182\mathrm{i}}_{T^{\mathrm{II}}-\mathrm{contribution}} \\ &= 0.4947 + 0.0196\mathrm{i}\,, \qquad (88) \end{aligned}$$

for $M_H = 250\,\mathrm{GeV}$. The second terms in the above two equations are the new physics corrections to the NLO Wilson coefficient $C_{7,\mathrm{SM}}(m_b)$, which is large and positive and makes the $a_7^p(K^*\gamma)$ positive also. The hard vertex and hard spectator contributions are also changed moderately, but have only small effects on the branching ratios.

For model III-B, the theoretical predictions for the branching ratios are

$$\begin{aligned} &\mathcal{B}(B \to \overline{K}^{*0}\gamma)^{\mathrm{III-B}} \\ &= \left[4.23^{+2.34}_{-1.83}(F_{K^*})^{+0.57}_{-0.37}(\mu)^{+0.05}_{-0.02}(\lambda_B) \pm 0.21(m_c)\right] \\ &\qquad \times 10^{-5} \\ &= \left(4.23^{+2.42}_{-1.88}\right) \times 10^{-5}\,, \qquad (89) \\ &\mathcal{B}(B \to K^{*-}\gamma)^{\mathrm{III-B}} \\ &= \left[5.07^{+2.66}_{-2.11}(F_{K^*})^{+0.44}_{-0.06})(\mu)^{+0.02}_{-0.05}(\lambda_B) \pm 0.24(m_c)\right] \\ &\qquad \times 10^{-5} \\ &= \left(5.07^{+2.71}_{-2.13}\right) \times 10^{-5}\,, \qquad (90) \end{aligned}$$

for $M_H = 250\,\mathrm{GeV}$.

Figure 6 shows the M_H dependence of the branching ratio $B \to K^*\gamma$ in model III-B. The dot-dashed and solid curves show the central value of the NLO model III-B prediction for the branching ratio $\mathcal{B}(B \to \overline{K}^{*0}\gamma)$ and $\mathcal{B}(B \to K^{*-}\gamma)$, respectively. Other bands or lines show the same thing as in Fig. 5.

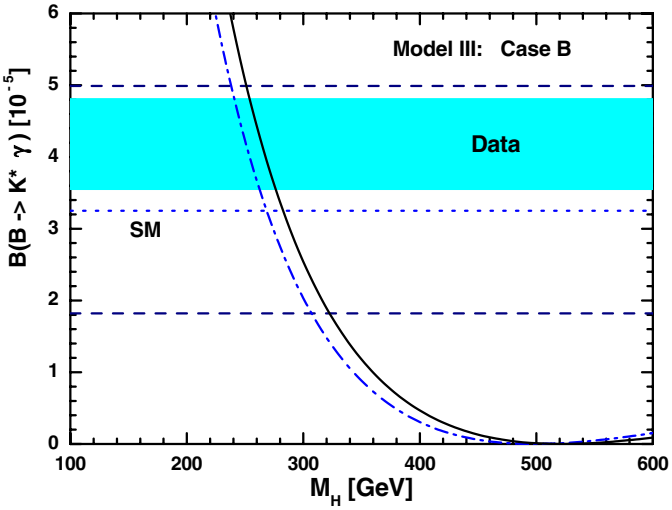

Fig. 6. The same as Fig. 5, but for model III-B, i.e. $(\lambda_{tt}, \lambda_{bb}) = (0.5, 22)$

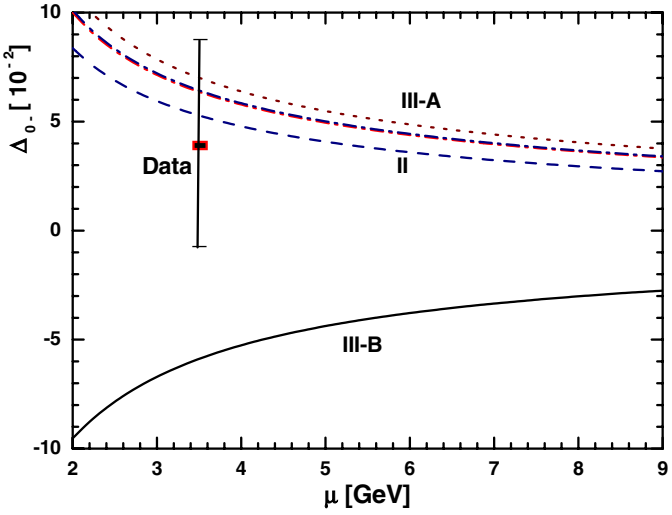

Fig. 7. The μ dependence of the isospin symmetry breaking $\Delta_{0-}(K^*\gamma)$ in the SM and the general 2HDM's. The error bar shows the data. For details see the text

If we add the theoretical errors as given in (89) and (90) with the corresponding experimental errors in (2) in quadrature and treat them as the total 1σ error, we then read off the allowed regions of M_H from Fig. 6:

$$218 \le M_H \le 293\,\text{GeV}, \quad \text{and} \quad M_H \ge 1670\,\text{GeV}\,, \quad (91)$$

allowed by the measured $\mathcal{B}(B \to \overline{K}^{*0}\gamma)$, and

$$226 \le M_H \le 315\,\text{GeV}, \quad \text{and} \quad M_H \ge 1490\,\text{GeV}\,, \quad (92)$$

allowed by the measured $\mathcal{B}(B \to K^{*-}\gamma)$. These constraints on M_H are well consistent with those obtained from the inclusive $B \to X_s\gamma$ decays as given in [13]. Of course, the large theoretical error is dominated by the uncertainty of the form factor F_{K^*} here.

For the exclusive $B \to K^*\gamma$ decay, the theoretical prediction for the CP symmetry $\mathcal{A}_{CP}$ as defined in (65) is very small:

$$|\mathcal{A}_{CP}(B \to K^*\gamma)| < 1\% \quad (93)$$

in the SM and all three types of the 2HDM's considered here, which is consistent with the measurements as reported by BaBar [15] and Belle Collaboration [16]:

$$\mathcal{A}_{CP}(B \to K^*\gamma) = [-0.17, +0.082]\,, \quad (94)$$

$$\mathcal{A}_{CP}(B \to K^*\gamma) = -0.001 \pm 0.044 \pm 0.008\,. \quad (95)$$

3.2 Isospin symmetry

As can be seen in the last subsection, the large uncertainty of the form factor F_{K^*} dominates the total error of the theoretical prediction of the branching ratios. For the isospin symmetry breaking of the $B \to K^*\gamma$ system, however, its dependence on the form factor F_{K^*} largely cancelled in the ratio. From (38) and (31), the isospin symmetry breaking $\Delta_{0-}(K^*\gamma)$ as defined in (66) can also be written as

$$\Delta_{0-}(K^*\gamma) = \frac{\eta_\tau |R_{\overline{K}^{*0}}|^2 - |R_{K^{*-}}|^2}{\eta_\tau |R_{\overline{K}^{*0}}|^2 + |R_{K^{*0}}|^2}\,, \quad (96)$$

where R_{K^*} have been given in (64). In our approximation, the isospin breaking is generated by weak annihilation contributions, and has a residue sensitivity to the form factors F_V induced through the F_V dependence of b^V and d^V functions as defined in (36) and (37). Since $\lambda_u^s = V_{us}^* V_{ub}$ is about two orders smaller than $\lambda_c^s = V_{cs}^* V_{cb}$, the function R_{K^*} is largely determined by $a_7^c(K^*\gamma)$.

In the SM, we have numerically

$$\begin{aligned}\Delta_{0-}(K^*\gamma)^{\rm SM} &= \left[5.6^{+1.7}_{-1.1}(F_{K^*})^{+4.0}_{-2.1}(\mu)^{+0.6}_{-1.4}(\lambda_B) \pm 0.1(m_c)\right] \times 10^{-2} \\ &= \left(5.6^{+4.4}_{-2.8}\right) \times 10^{-2}\,, \end{aligned} \quad (97)$$

where the errors are added in quadrature. The dominant error comes from the uncertainty of the low energy scale $1/2m_b \le \mu \le 2m_b$. The SM prediction agrees well with the measured value of $\Delta_{0-}^{\rm exp}(K^*\gamma) = (3.9 \pm 4.8)\%$.

In general two-Higgs-doublet models, by assuming $\tan\beta = 4$ and $M_H = 250\,\text{GeV}$, we find numerically

$$\Delta_{0-}(K^*\gamma)^{\rm I} = \left(+5.7^{+4.3}_{-2.7}\right) \times 10^{-2}\,, \quad (98)$$

$$\Delta_{0-}(K^*\gamma)^{\rm II} = \left(+4.6^{+3.7}_{-2.4}\right) \times 10^{-2}\,, \quad (99)$$

$$\Delta_{0-}(K^*\gamma)^{\rm III-A} = \left(+6.2^{+4.7}_{-3.0}\right) \times 10^{-2}\,, \quad (100)$$

$$\Delta_{0-}(K^*\gamma)^{\rm III-B} = \left(-5.1^{+2.6}_{-4.3}\right) \times 10^{-2}\,, \quad (101)$$

where the errors induced by the uncertainties of μ, F_{K^*}, λ_B and m_c have been added in quadrature, and the uncertainty of μ dominates the total theoretical error.

Figure 7 shows the μ dependence of the isospin symmetry breaking $\Delta_{0-}(K^*\gamma)$ in the general 2HDM's for $\tan\beta = 4$ and $M_H = 250\,\text{GeV}$. The two coinciding dot-dashed curves show the SM and model I prediction, the dash and dots curve show the model II and model III-A prediction respectively, and the solid curve refers to the model III-B prediction. The error bar shows the data $\Delta_{0-}(K^*\gamma)^{\rm exp} = (3.9 \pm 4.8)\%$.

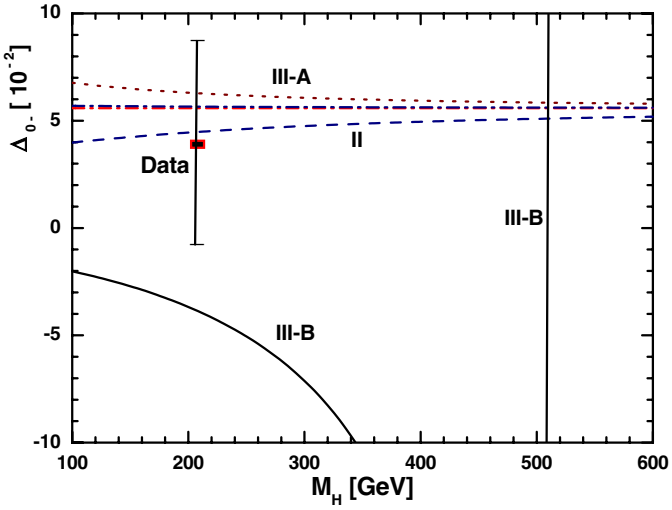

Fig. 8. The M_H dependence of the isospin symmetry breaking $\Delta_{0-}(K^*\gamma)$ in the SM and the general 2HDM's. The error bar shows the data. For details see the text

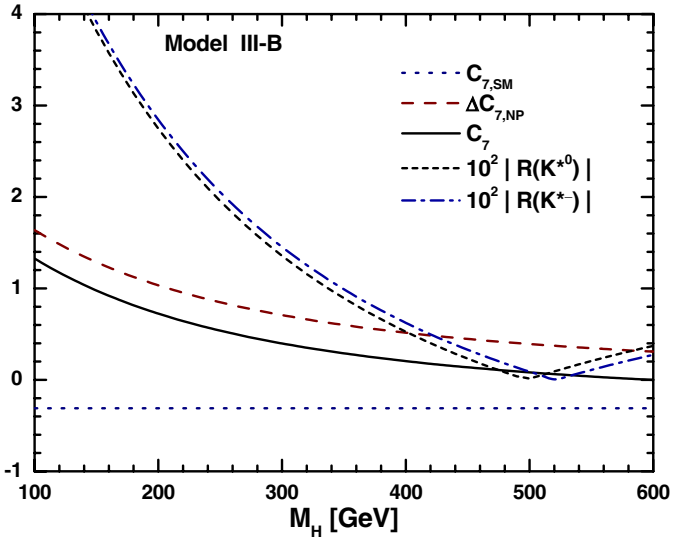

Fig. 9. Plots of the M_H dependence of $C_{7,\mathrm{SM}}(m_b)$ (horizontal dots line), $\Delta C_{7,\mathrm{NP}}$ (dashed curve), $C_7(m_b)$ (solid curve), $10^2|R(\overline{K}^{*0}\gamma)|$ (short-dashed curve) and $10^2|R(K^{*-}\gamma)|$ (dot-dashed curve)

Figure 8 shows the M_H dependence of the isospin symmetry breaking $\Delta_{0-}(K^*\gamma)$ in the general 2HDM's for $\tan\beta = 4$ and $\mu = m_b$ GeV. The two coinciding dot-dashed curves show the SM and model I predictions. The dashed and dots solid curves show the model II, III-A and III-B predictions, respectively. The error bar shows the data as in Fig. 7.

From the above two figures, one can see that only the theoretical prediction of the model III-B is rather different from that of the SM and looks like deviating from the data. But the regions $M_H < 200\,\mathrm{GeV}$ and $300 \lesssim M_H \lesssim 1500\,\mathrm{GeV}$ have been excluded by the data of inclusive $B \to X_s\gamma$ [13] and by the constraint as illustrated in Fig. 6. The main reason for the great changes of the solid curve in Fig. 8 is the strong cancellation between the negative $C_{7,\mathrm{SM}}(m_b)$ and its positive new physics counterpart as illustrated clearly in Fig. 9, where the solid curve shows the summation of the SM and new physics contributions to the dominant Wilson coefficient C_7, i.e., $C_7(m_b) = C_{7,\mathrm{SM}}(m_b) + \Delta C_{7,\mathrm{NP}}(m_b)$. When $C_7(m_b)$ approaches zero, the summation of other "originally small" parts (such as the T_i^{I}, T_i^{II} and a_{ann}^p contributions) becomes important and leads to an abnormally large isospin breaking. The short-dashed and dot-dashed curves in Fig. 9 shows the absolute value of $R_{\overline{K}^{*0}}$ and $R_{K^{*-}}$, respectively. The isospin breaking is proportional to the difference of their squares. At the close region of the crossing point of $R_{\overline{K}^{*0}}$ and $R_{K^{*-}}$, the ratio $\Delta_{0-}(K^*\gamma)$ can be large and changes sign. But as mentioned previously, this region around $M_H = 500\,\mathrm{GeV}$ has been excluded by the data of the branching ratios from both the inclusive and exclusive radiative B meson decays.

In the region of $M_H \sim 250\,\mathrm{GeV}$, model III-B is disfavored by the measured value of isospin breaking $\Delta_{0-}(K^*\gamma)$ as can be seen from Figs. 7 and 8. But taking the sizable experimental and theoretical uncertainties into account, the theoretical prediction of model III-B is still compatible with the data within 2σ errors. In other words, the positive $C_7(m_b)$ is disfavored but cannot be excluded by the present data.

4 $B \to \rho\gamma$

When compared with $B \to K^*\gamma$ decay, the $B \to \rho\gamma$ decay mode is particularly interesting in the search for new physics beyond the SM, because of the suppression of $b \to d$ transitions in the SM and the simultaneous chirality suppression. For $B \to \rho\gamma$ decay, we generally know that
(a) both a_7^u and a_7^c contribute effectively since λ_u^d and λ_c^d are comparable in magnitude;
(b) the branching ratios of $B \to \rho\gamma$ are suppressed with respect to $B \to K^*\gamma$ by roughly a factor of $|V_{td}/V_{ts}|^2 \approx 4 \times 10^{-2}$;
(c) the CP asymmetry $\mathcal{A}_{CP}(B \to \rho\gamma)$ is generally at 10% level, and may be observed in B factory experiments;
(d) the new physics may provide a significant contribution to the observables of $B \to \rho\gamma$ decay;
(e) only the experimental upper limits on the branching ratios of $B \to \rho\gamma$ are available now.

4.1 Branching ratios and CP asymmetries

From (38), the branching ratios of $B \to \rho\gamma$ decays can be written as

$$\mathcal{B}(\overline{B} \to \rho\gamma) = \tau_B \frac{G_{\mathrm{F}}^2 \alpha m_B^3 m_b^2}{32\pi^4} \left(1 - \frac{m_\rho^2}{m_B^2}\right)^3 |R_\rho|^2 c_\rho^2 |F_\rho|^2, \tag{102}$$

with

$$R_\rho = V_{ud}^* V_{ub}\, [a_7^u(\rho\gamma) + a_{\mathrm{ann}}^u(\rho\gamma)]$$

$$+ V_{cd}^* V_{cb} \left[a_7^c(\rho\gamma) + a_{\rm ann}^c(\rho\gamma)\right] . \qquad (103)$$

By using the formulas as given in (32) and (34) and the central values of the input parameters in Table 3, we find the SM predictions for $a_7^p(\rho\gamma)$ and $a_{\rm ann}(\rho\gamma)$ at the low energy scale $\mu = m_b$,

$$\begin{aligned} a_7^u(\rho\gamma) &= \underbrace{-0.3212}_{C_{7,\rm SM}^0(m_b)} + \underbrace{0.0113}_{\Delta C_{7,\rm SM}^1} \underbrace{-0.1407 - 0.0683{\rm i}}_{T^{\rm I}-\text{contribution}} \\ &\quad \underbrace{+0.0343 - 0.0003{\rm i}}_{T^{\rm II}-\text{contribution}} \\ &= -0.4164 - 0.0686{\rm i}\,, \qquad (104) \\ a_7^c(\rho\gamma) &= \underbrace{-0.3212}_{C_{7,\rm SM}^0(m_b)} + \underbrace{0.0113}_{\Delta C_{7,\rm SM}^1} \underbrace{-0.0802 - 0.0131{\rm i}}_{T^{\rm I}-\text{contribution}} \\ &\quad \underbrace{-0.0166 - 0.0143{\rm i}}_{T^{\rm II}-\text{contribution}} \\ &= -0.4067 - 0.0274{\rm i}\,, \qquad (105) \\ a_{\rm ann}^u(\rho^0\gamma) &= -0.0032, \quad a_{\rm ann}^c(\rho^0\gamma) = -0.0127, \\ a_{\rm ann}^u(\rho^-\gamma) &= 0.1883, \quad a_{\rm ann}^c(\rho^-\gamma) = 0.0032\,. \qquad (106) \end{aligned}$$

Here the values of the weak annihilation factors are slightly different from those for $B \to K^*\gamma$ decay, and only the $T^{\rm II}$ contributions to $a_7^p(\rho\gamma)$ are different from those to $a_7^p(K^*\gamma)$ because of the small differences of the H_i functions between two decay modes as can be seen in Appendix A.

The corresponding NLO SM predictions for the branching ratio $\mathcal{B}(B \to \rho\gamma)$ are

$$\begin{aligned} &\mathcal{B}(B \to \rho^0\gamma)^{\rm SM} \\ &= \left[0.91 \pm 0.29(\gamma)^{+0.25}_{-0.22}(F_\rho) \pm 0.17(\mu)^{+0.10}_{-0.03}(\lambda_B)\right. \\ &\quad \left. \pm 0.10(m_c)\right] \times 10^{-6} \\ &= \left(0.91^{+0.42}_{-0.40}\right) \times 10^{-6}\,, \qquad (107) \\ &\mathcal{B}(B \to \rho^-\gamma)^{\rm SM} \\ &= \left[2.03 \pm 0.34(\gamma)^{+0.54}_{-0.47}(F_\rho) \pm 0.31(\mu)^{+0.46}_{-0.13}(\lambda_B)\right. \\ &\quad \left. \pm\, 0.12(m_c)\right] \times 10^{-6} \\ &= \left(2.03^{+0.85}_{-0.67}\right) \times 10^{-6}\,, \qquad (108) \end{aligned}$$

where the individual errors have been added in quadrature. The uncertainties of the CKM angle γ (here we take $\gamma = (60 \pm 20)^\circ$ in the calculation) and the form factor F_ρ dominate the total error, and the remaining errors from the other input parameters are negligibly small.

The central values and theoretical uncertainties of the branching ratios $\mathcal{B}(B \to \rho\gamma)$ in the SM and the general 2HDM's are all listed in Table 4. The SM prediction is well consistent with the experimental upper limits within 1σ error. The predictions of model I, II and III-A are also compatible with the data within errors, as illustrated in Figs. 10 and 11 for $B \to \rho^0\gamma$ and $B \to \rho^-\gamma$, respectively. For model III-B, however, the branching ratios can be changed significantly when the charged Higgs boson is light or heavy,

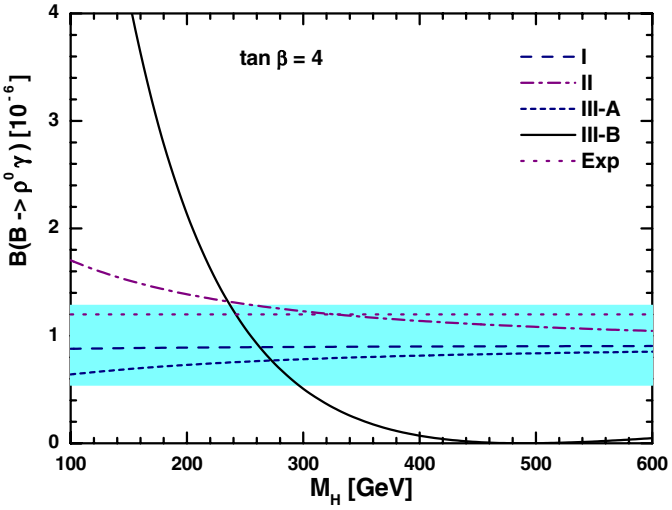

Fig. 10. Plots of the M_H dependence of the branching ratio $B \to \rho^0\gamma$ in the SM (shaded band), model I and II (dashed and dot-dashed curves), and model III-A (short-dashed curve) and III-B (solid curve). The horizontal dots line shows the experimental upper bound (at 9% C.L. [15]): $\mathcal{B}(B \to \rho^0\gamma) < 1.2 \times 10^{-6}$

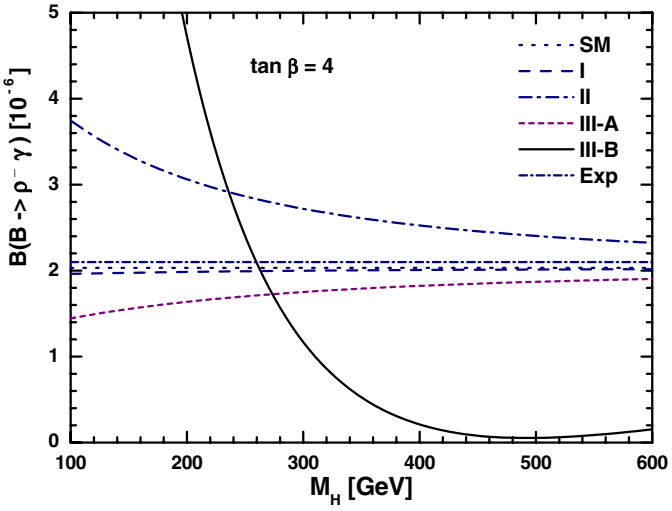

Fig. 11. The same as Fig. 10, but for the decay $B \to \rho^-\gamma$

as illustrated by the solid curves in Figs. 10 and 11. From the experimental upper bounds on $\mathcal{B}(B \to \rho\gamma)$ as given in Table 1, we find the lower limit on M_H:

$$M_H \geq 206\,{\rm GeV} \qquad (109)$$

when the 2σ theoretical errors are also taken into account. This lower bound is compatible with those obtained from the measured $\mathcal{B}(B \to K^*\gamma)$ as given in (91) and (92) and from the inclusive $B \to X_s\gamma$ decay [13].

The CP asymmetry of $B \to \rho\gamma$ decays is defined in the same way as for $B \to K^*\gamma$ decays in (65). Using the input parameters as listed in Table 3, one finds the NLO SM predictions:

Table 4. The NLO theoretical predictions for branching ratios and CP asymmetries in the SM and models I, II, III-A and III-B, assuming $\tan\beta = 4$ and $M_H = 250\,\text{GeV}$. The errors induced by the uncertainties of six input parameters ($\mu, R_b, \lambda_B, m_c, F_\rho$ and γ) are taken into account. Individual errors are added in quadrature

Decays	SM	Model I	Model II	Model III-A	Model III-B
$\mathcal{B}(\overline{B}^0 \to \rho^0\gamma)$ (10^{-6})	$0.91^{+0.42}_{-0.40}$	$0.90^{+0.41}_{-0.39}$	$1.30^{+0.59}_{-0.51}$	$0.76^{+0.35}_{-0.33}$	$1.07^{+0.50}_{-0.41}$
$\mathcal{B}(B^- \to \rho^-\gamma)$ (10^{-6})	$2.0^{+0.8}_{-0.7}$	$2.0^{+0.8}_{-0.7}$	$2.9^{+1.2}_{-0.9}$	$1.7^{+0.7}_{-0.6}$	$2.4^{+1.4}_{-1.1}$
$\mathcal{A}_{CP}(\overline{B}^0 \to \rho^0\gamma)$ (%)	$8.4^{+4.4}_{-3.2}$	$8.5^{+4.4}_{-3.5}$	$7.0^{+3.8}_{-3.0}$	$9.3^{+4.8}_{-3.9}$	$-7.2^{+3.6}_{-4.6}$
$\mathcal{A}_{CP}(B^- \to \rho^-\gamma)$ (%)	$10.4^{+6.0}_{-3.8}$	$10.5^{+6.0}_{-3.9}$	$8.7^{+5.1}_{-2.7}$	$11.4^{+6.5}_{-3.9}$	$-8.5^{+4.2}_{-5.0}$

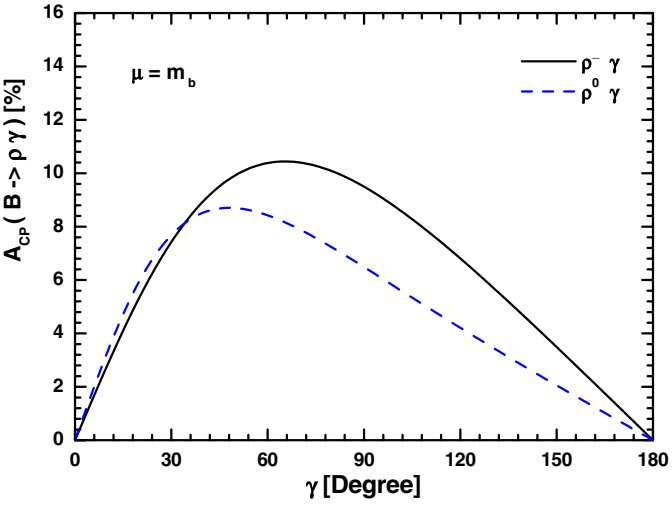

Fig. 12. Plots of the angle γ dependence of the CP asymmetries for $B \to \rho^0\gamma$ (dashed curve) and $B^\pm \to \rho^\pm\gamma$ (solid curve) decays in the SM

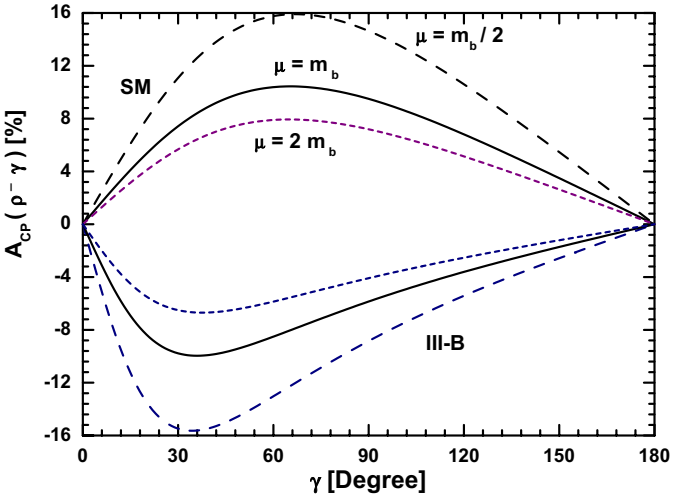

Fig. 13. Plots of the angle γ dependence of the CP asymmetry for $B^\pm \to \rho^\pm\gamma$ decay in the SM and model III-B for $\mu = m_b/2$ (dots curves), m_b (solid curves) and $2m_b$ (dashed curves)

$$
\begin{aligned}
&\mathcal{A}_{CP}(\rho^0\gamma)^{\rm SM} \\
&= \left[8.4^{+3.8}_{-1.8}(\mu) \pm 1.9(R_b) \pm 0.8(\lambda_B)^{+0.9}_{-1.1}(m_c)\right. \\
&\qquad \left. \pm 0.4(F_\rho)^{+0.1}_{-1.2}(\gamma)\right] \times 10^{-2} \\
&= \left(8.4^{+4.4}_{-3.2}\right) \times 10^{-2}\,, \qquad (110) \\
&\mathcal{A}_{CP}(\rho^\pm\gamma)^{\rm SM} \\
&= \left[10.4^{+5.4}_{-2.5}(\mu) \pm 2.4(R_b)^{+0.3}_{-0.0}(\lambda_B) \pm 0.8(m_c)\right. \\
&\qquad \left. \pm\, 0.1(F_\rho)^{-0.3}_{-1.4}(\gamma)\right] \times 10^{-2} \\
&= \left(10.4^{+6.0}_{-3.8}\right) \times 10^{-2}\,, \qquad (111)
\end{aligned}
$$

where the errors have been added in quadrature. The CP asymmetry of $B \to \rho\gamma$ is large in size and depends sensitively on the variations of the scale μ and $R_b = \sqrt{\bar\rho^2 + \bar\eta^2}$. If we consider the whole range of $0^\circ \le \gamma \le 180^\circ$ instead of $\gamma = (60 \pm 20)^\circ$ preferred by the global fit result [31], the CP asymmetry $\mathcal{A}_{CP}(B \to \rho\gamma)$ also shows a strong dependence on the angle γ as illustrated by Fig. 12 for $B^\pm \to \rho^\pm\gamma$ (solid curve) and $B \to \rho^0\gamma$ (dashed curve) decays.

The numerical values of CP asymmetries in the SM and the general 2HDM's are also listed in Table 4. The theoretical predictions of the SM and models I, II and III-A are all compatible, around +10%. The CP asymmetry $\mathcal{A}_{CP}(B \to \rho\gamma)$ in model III-B, however, is comparable in size with the SM prediction, but has an opposite sign, as shown in Fig. 13, where the upper and lower three curves show the theoretical predictions for $\mu = m_b/2$ (dashed curves), m_b (solid curves) and $2m_b$ (dots curves) in the SM and model III-B, respectively. For the $B \to \rho^0\gamma$ decay mode, we have a similar conclusion. This feature may serve as a good observable to distinguish model III-B (or a positive $C_7(m_b)$) with the SM (a negative $C_7(m_b)$).

4.2 Isospin and U-spin symmetries

According to currently available data, the $SU(2)$ isospin symmetry of the strong interaction is a very good symmetry with a breaking of no more than 5%. The U-spin symmetry, the $SU(3)$ flavor symmetry of the strong interaction under exchanges of the down and strange quarks, however, may have a breaking of around 20% (i.e., $\sim (F_K/F_\pi - 1)$) as frequently used in the study of $B \to K\pi$ decays. For the exclusive $B \to K^*\gamma$ decays, the isospin breaking derived from the measured branching ratios is indeed around 5% as given in (67). For $B \to \rho\gamma$ decays, no measurements are available now.

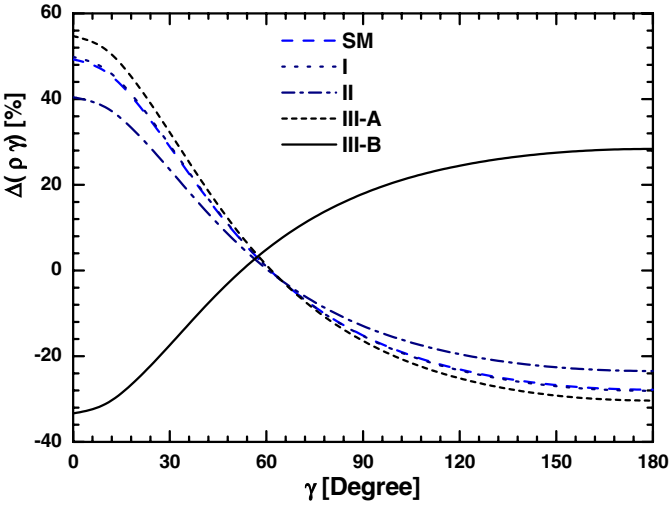

Fig. 14. The isospin breaking $\Delta(\rho\gamma)$ versus the CKM angle γ in the SM and general 2HDM's for $\tan\beta = 4$ and $M_H = 250\,\text{GeV}$

As in [24,26], we also define the isospin symmetry breaking of $B \to \rho\gamma$ decays in the form of

$$\Delta(\rho\gamma) = \frac{1}{2}\left[\frac{\Gamma(B^+ \to \rho^+\gamma)}{2\Gamma(B^0 \to \rho^0\gamma)} + \frac{\Gamma(B^+ \to \rho^+\gamma)}{2\Gamma(B^0 \to \rho^0\gamma)} - 2\right]. \tag{112}$$

Using the central values of input parameters as listed in Table 3 and assuming $\tan\beta = 4$, $M_H = 250\,\text{GeV}$, we find numerically that

$$\Delta(\rho\gamma) = \begin{cases} \left(0.9^{+23.3}_{-13.5}\right) \times 10^{-2} & \text{in SM}\,, \\ \left(0.9^{+23.3}_{-13.6}\right) \times 10^{-2} & \text{in model I}\,, \\ \left(0.4^{+18.3}_{-11.1}\right) \times 10^{-2} & \text{in model II}\,, \\ \left(1.3^{+25.9}_{-14.9}\right) \times 10^{-2} & \text{in model III-A}\,, \\ \left(4.9^{+12.0}_{-14.6}\right) \times 10^{-2} & \text{in model III-B}\,, \end{cases} \tag{113}$$

where the errors from the uncertainties of the input parameters have been added in quadrature. The largest theoretical uncertainty comes from the CKM angle γ.

In Fig. 14, we show the angle γ dependence of the isospin breaking $\Delta(\rho\gamma)$ in the SM and the considered 2HDM's for $\tan\beta = 4$, $M_H = 250\,\text{GeV}$ and $0^\circ \le \gamma \le 180^\circ$. It is easy to see from Fig. 14 that

(a) except for model III-B, the isospin breaking in the SM and other 2HDM's have a similar γ dependence;

(b) all theoretical predictions become almost identical and very small in magnitude for $\gamma \sim 55^\circ$(the value preferred by the global fit results), and the smallness of $\Delta(\rho\gamma)$ is also consistent with the general expectation and other measurements;

(c) the theoretical predictions in the SM and model III-B have a very different γ dependence, and have the opposite sign for small or large values of the CKM angle γ.

The U-spin symmetry is another interesting observable for $B \to (K^*, \rho)\gamma$ decays, and has been studied for example in [24,26,45]. In the limit of U-spin symmetry, the quantity

$$\Delta U(K^*, \rho) \equiv \Delta\mathcal{B}(B \to K^*\gamma) + \Delta\mathcal{B}(B \to \rho\gamma) \equiv 0, \tag{114}$$

with

$$\Delta\mathcal{B}(B \to K^*\gamma) = \mathcal{B}(B^+ \to K^{*+}\gamma) - \mathcal{B}(B^- \to K^{*-}\gamma), \tag{115}$$

$$\Delta\mathcal{B}(B \to \rho\gamma) = \mathcal{B}(B^+ \to \rho^+\gamma) - \mathcal{B}(B^- \to \rho^-\gamma) \tag{116}$$

should be satisfied. Using the central values of the input parameters, we find the SM prediction of $\Delta U(K^*, \rho)$

$$\Delta\mathcal{B}(B \to K^*\gamma) = -3.7 \times 10^{-7}\,, \tag{117}$$

$$\Delta\mathcal{B}(B \to \rho\gamma) = +4.4 \times 10^{-7}\,, \tag{118}$$

where we have chosen $\gamma = 90^\circ$ which maximizes the effects. The two parts have opposite signs and cancel to a large extent, leaving a small U-spin breaking:

$$\Delta U(K^*, \rho) = 0.7 \times 10^{-7} \tag{119}$$

in the SM, which is only about 8% of $\mathcal{B}(B \to \rho^0\gamma)$. In the general 2HDM's, we find the numerical results

$$\Delta U(K^*, \rho) = \begin{cases} 0.7 \times 10^{-7} & \text{in model I}\,, \\ 0.9 \times 10^{-7} & \text{in model II}\,, \\ 0.6 \times 10^{-7} & \text{in model III-A}\,, \\ -1.5 \times 10^{-7} & \text{in model III-B}\,, \end{cases} \tag{120}$$

for $\tan\beta = 4$, $M_H = 250\,\text{GeV}$ and $\gamma = 90^\circ$. The new physics contributions in the conventional model I, II and model III-A have little effect on the size of U-spin symmetry breaking. In model III-B, although $\Delta U(K^*, \rho)$ becomes negative, it is still small in magnitude.

5 Conclusions

By employing the QCD factorization approach for the exclusive $B \to V\gamma$ decays as proposed in [22–24], we calculated the NLO new physics contributions to the branching ratios, CP asymmetries, isospin symmetry breaking and U-spin symmetry breaking of the exclusive radiative decays $B \to K^*\gamma$ and $B \to \rho\gamma$, induced by the charged Higgs penguin diagrams appearing in general two-Higgs-doublet models including the conventional model I and II, as well as the two typical cases of model III. The NLO new physics contributions are included through their corrections to the NLO Wilson coefficients $C_7(M_W)$ and $C_8(M_W)$ at the matching scale M_W.

In Sect. 2, we gave a brief review of the effective Hamiltonian and the calculation of the exclusive $B \to V\gamma$ ($V = K^*, \rho$) decays at next-to-leading order in QCD factorization, and we presented the relevant formulas for the calculation of Wilson coefficients and physical observables in the SM and the general two-Higgs-doublet models.

In Sects. 3 and 4, we calculated the NLO new physics contributions to the branching ratios and other observables of $B \to K^*\gamma$ and $B \to \rho\gamma$ decays in the general 2HDM's, compared the theoretical predictions with those currently available in experimental measurements, and found the following points.

(1) The new physics corrections to the physical observables under consideration in this paper are generally small in model I and model III-A, moderate in model II, but large in model III-B. And therefore the theoretical predictions in the SM, model I and III-A are always in good agreement with the corresponding data.

(2) For model II, a lower bound on the mass M_H can be obtained from the measured branching ratios of $B \to K^*\gamma$ decays:

$$M_H \gtrsim 200 \quad \text{or} \quad 300\,\text{GeV}, \tag{121}$$

if one uses $F_{K^*} = 0.25 \pm 0.06$ or $F_{K^*} = 0.38 \pm 0.06$ in the calculation, as illustrated by Figs. 2 and 4. From Fig. 3, a lower limit of $\tan\beta > 0.5$ can also be obtained from the data.

(3) In model III-B, the new physics contributions to $C_{7,8}(M_W)$ are larger than their SM counterparts in size and they change the sign of the dominant Wilson coefficient $C_7(m_b)$ from negative to positive, as given in (87) and (88).

(4) In model III-B, the ranges of

$$226 \le M_H \le 293\,\text{GeV} \quad \text{and} \quad M_H \ge 1670\,\text{GeV} \tag{122}$$

are still allowed by the measured $\mathcal{B}(B \to K^*\gamma)$ as given in (2). From the experimental upper bounds on $\mathcal{B}(B \to \rho\gamma)$, we find the lower limit on M_H

$$M_H \ge 206\,\text{GeV}, \tag{123}$$

when the 2σ theoretical errors are also taken into account. The above limits on M_H are comparable with those obtained from the inclusive $B \to X_s\gamma$ decay [13].

(5) The model III-B prediction for the isospin symmetry breaking of $B \to K^*\gamma$ decay is $\Delta_{0-}(K^*\gamma) = (-5.6^{+4.4}_{-2.8})\%$, which is small in size but has a sign opposite to the measured value, as illustrated in Figs. 7 and 8. A positive $C_7(m_b)$ is therefore disfavored by the measured value of $\Delta_{0-}^{\text{exp}}(K^*\gamma) = (3.9 \pm 4.8)\%$, but it still cannot be excluded if we take the large theoretical and experimental errors into account.

(6) The theoretical predictions for the CP asymmetry $\mathcal{A}_{CP}(B \to K^*\gamma)$ is always less than one percent in magnitude in the SM and all three types of general 2HDM's considered here. For $B \to \rho\gamma$ decay, however, its CP asymmetry can be as large as about 10% in size in the SM and all three types of 2HDM's and have a strong dependence on the variations of the scale $\mu = \mathcal{O}(m_b)$ and the CKM angle γ, as shown in Figs. 12 and 13. It is interesting to see from Fig. 13 that the CP asymmetry in model III-B has an opposite sign to the one in the SM. This feature may be used as a good observable to distinguish model III-B (or a positive $C_7(m_b)$) with the SM (a negative $C_7(m_b)$).

(7) For $B \to \rho\gamma$ decay, the isospin symmetry breaking is less than 10% in the region of $\gamma = [40 \sim 70]^\circ$ as preferred by the global fit result [31], but can be as large as 20 to 40% in the regions of $\gamma \le 10^\circ$ and $\gamma \ge 120^\circ$, as can be seen clearly in Fig. 14. The SM and model III-B predictions for isospin breaking have an opposite sign for small or large values of the CKM angle γ.

(8) The U-spin symmetry breaking $\Delta U(K^*, \rho)$ in the SM and all 2HDM's considered here is generally small in size: $\sim 10^{-7}$.

Acknowledgements. Z.J. Xiao is very grateful to the high energy section of ICTP, Italy, where part of this work was done, for warm hospitality and financial support. This work was supported by the National Natural Science Foundation of China under Grant No. 10075013 and 10275035, and by the Research Foundation of Nanjing Normal University under Grant No. 214080A916.

A G_i and H_i^V functions

In this appendix, the explicit expressions or numerical values of all G_i and H_i^V functions appearing in (30) will be listed. For more details of these functions, see [26] and references therein. We have

$$G_1(z) = \frac{52}{81}\ln\frac{\mu}{m_b} + \frac{833}{972} - \frac{1}{4}[a(z) + b(z)] + \frac{10\mathrm{i}\pi}{81}, \tag{A.1}$$

$$G_2(z) = -\frac{104}{27}\ln\frac{\mu}{m_b} - \frac{833}{162} + \frac{3}{2}[a(z) + b(z)] - \frac{20\mathrm{i}\pi}{27}, \tag{A.2}$$

$$G_3 = \frac{44}{27}\ln\frac{\mu}{m_b} + \frac{598}{81} + \frac{2\pi}{\sqrt{3}} + \frac{8}{3}X_b - \frac{3}{4}a(1) + \frac{3}{2}b(1) + \frac{14\mathrm{i}\pi}{27}, \tag{A.3}$$

$$G_4(z_c) = \frac{38}{81}\ln\frac{\mu}{m_b} + -\frac{761}{972} - \frac{\pi}{3\sqrt{3}} - \frac{4}{9}X_b + \frac{1}{8}a(1) + \frac{5}{4}b(z_c) - \frac{37\mathrm{i}\pi}{81}, \tag{A.4}$$

$$G_5 = \frac{1568}{27}\ln\frac{\mu}{m_b} + \frac{14170}{81} + \frac{8\pi}{\sqrt{3}} + \frac{32}{3}X_b - 12a(1) + 24b(1) + \frac{224\mathrm{i}\pi}{27}, \tag{A.5}$$

$$G_6(z_c) = -\frac{1156}{81}\ln\frac{\mu}{m_b} + \frac{2855}{486} - \frac{4\pi}{3\sqrt{3}} - \frac{16}{9}X_b - \frac{5}{2}a(1) + 11b(1) + 9a(z_c) + 15b(z_c) - \frac{574\mathrm{i}\pi}{81}, \tag{A.6}$$

$$G_8 = \frac{8}{3}\ln\frac{\mu}{m_b} + \frac{11}{3} - \frac{2\pi^2}{9} + \frac{2\mathrm{i}\pi}{3}, \tag{A.7}$$

where

$$X_b = \int_0^1 \mathrm{d}x \int_0^1 \mathrm{d}y \int_0^1 \mathrm{d}v$$

$$\times xy \ln[v + x(1-x)(1-v)(1-v+vy)]$$
$$\approx -0.1684, \tag{A.8}$$

$$a(1) \simeq 4.0859 + \frac{4\mathrm{i}\pi}{9}, \tag{A.9}$$

$$b(1) = \frac{320}{81} - \frac{4\pi}{3\sqrt{3}} + \frac{632\pi^2}{1215} - \frac{8}{45}\left[\frac{\mathrm{d}^2 \ln \Gamma(x)}{\mathrm{d}x^2}\right]_{x=\frac{1}{6}}$$
$$+ \frac{4\mathrm{i}\pi}{81} \simeq 0.0316 + \frac{4\mathrm{i}\pi}{81}, \tag{A.10}$$

$$a(z_u) = (-1.93 + 4.96\mathrm{i}) \times 10^{-5}, \tag{A.11}$$

$$a(z_c) = 1.525 + 1.242\mathrm{i}, \tag{A.12}$$

$$b(z_u) = (1.11 + 0.28\mathrm{i}) \times 10^{-5}, \tag{A.13}$$

$$b(z_c) = -0.0195 + 0.1318\mathrm{i}, \tag{A.14}$$

where $z_q = m_q^2/m_b^2$ and the masses m_q ($q = u, c, b$) as listed in Table 3 have been used to obtain the numerical results. The explicit analytical expressions for $a(z)$ and $b(z)$ can be found for example in [26].

For the H_i^V functions, we have

$$H_1^V(z_p) = -\frac{2\pi^2}{9}\frac{f_B f_V^\perp \lambda_B}{F_V m_B}\int_0^1 \mathrm{d}v\, h(\bar{v}, z_p)\Phi_V^\perp(v), \tag{A.15}$$

$$H_2^V = 0, \tag{A.16}$$

$$H_3^V = -\frac{1}{2}\left[H_1^V(1) + H_1^V(0)\right], \tag{A.17}$$

$$H_4^V(z_c) = H_1^V(z_c) - \frac{1}{2}H_1^V(1), \tag{A.18}$$

$$H_5^V = 2H_1^V(1), \tag{A.19}$$

$$H_6^V(z_c) = -H_1^V(z_c) + \frac{1}{2}H_1^V(1) = -H_4^V(z_c), \tag{A.20}$$

$$H_8^V = -\frac{4\pi^2}{3}\frac{f_B f_V^\perp \lambda_B}{F_V m_B}\left(1 - \alpha_1^V + \alpha_2^V + \ldots\right), \tag{A.21}$$

where the hard-scattering function $h(u, z)$ is given by

$$h(u,z) = \frac{4z}{u^2}\left\{\mathrm{Li}_2\left[\frac{2}{1-\sqrt{\frac{u-4z+\mathrm{i}\varepsilon}{u}}}\right] + \mathrm{Li}_2\left[\frac{2}{1+\sqrt{\frac{u-4z+\mathrm{i}\varepsilon}{u}}}\right]\right\} - \frac{2}{u}, \tag{A.22}$$

where $\mathrm{Li}_2[x]$ is the dilogarithmic function, and the function $h(u, z)$ is real for $u \le 4z$ and develops an imaginary part for $u > 4z$. The light-cone wave function $\Phi_V^\perp(v)$ takes the form of

$$\Phi_V^\perp(v) = 6v(1-v) \times \left[1 + \alpha_1^V(\mu)C_1^{3/2}(2v-1) + \alpha_2^V(\mu)C_2^{3/2}(2v-1) + \ldots\right], \tag{A.23}$$

where $C_1^{3/2}(x) = 3x$, $C_2^{3/2}(x) = \frac{3}{2}(5x^2-1)$.

B NLO coefficients at $\mu = M_W$ in general 2HDM's

For completeness, we list here the expressions of the NLO functions $W_{i,j}, M_{i,j}$ and $T_{i,j}$ ($i = 7, 8$ and $j = YY, XY$) at the matching scale $\mu_W = M_W$ in the general two-Higgs-doublet models. For more details see [37].

The NLO functions proportional to the term $|Y|^2$ are

$$W_{7,YY}(y) = \frac{2y}{9}\left[\frac{8y^3 - 37y^2 + 18y}{(y-1)^4}\mathrm{Li}_2\left(1-\frac{1}{y}\right) + \frac{3y^3 + 23y^2 - 14y}{(y-1)^5}\ln^2 y + \frac{21y^4 - 192y^3 - 174y^2 + 251y - 50}{9(y-1)^5}\ln y + \frac{-1202y^3 + 7569y^2 - 5436y + 797}{108(y-1)^4}\right] - \frac{4}{9}E_H, \tag{B.1}$$

$$W_{8,YY}(y) = \frac{y}{6}\left[\frac{13y^3 - 17y^2 + 30y}{(y-1)^4}\mathrm{Li}_2\left(1-\frac{1}{y}\right) - \frac{17y^2 + 31y}{(y-1)^5}\ln^2 y + \frac{42y^4 + 318y^3 + 1353y^2 + 817y - 226}{36(y-1)^5}\ln y + \frac{-4451y^3 + 7650y^2 - 18153y + 1130}{216(y-1)^4}\right] - \frac{1}{6}E_H, \tag{B.2}$$

$$M_{7,YY}(y) = \frac{y}{27}\left[\frac{-14y^4 + 149y^3 - 153y^2 - 13y + 31 - (18y^3 + 138y^2 - 84y)\ln y}{(y-1)^5}\right], \tag{B.3}$$

$$M_{8,YY}(y) = \frac{y}{36}\left[\frac{-7y^4 + 25y^3 - 279y^2 + 223y + 38 + (102y^2 + 186y)\ln y}{(y-1)^5}\right], \tag{B.4}$$

$$T_{7,YY}(y) = \frac{y}{9}\left[\frac{47y^3 - 63y^2 + 9y + 7 - (18y^3 + 30y^2 - 24y)\ln y}{(y-1)^5}\right], \tag{B.5}$$

$$T_{8,YY}(y) = \frac{2y}{3}\left[\frac{-y^3 - 9y^2 + 9y + 1 + (6y^2 + 6y)\ln y}{(y-1)^5}\right], \tag{B.6}$$

with

$$E_H(y) = \frac{y}{36} \tag{B.7}$$

$$\times \left[\frac{7y^3 - 36y^2 + 45y - 16 + (18y-12)\ln y}{(y-1)^4}\right].$$

The NLO functions proportional to the term (XY^*) are

$$W_{7,XY}(y) = \frac{4y}{3}\left[\frac{8y^2-28y+12}{3(y-1)^3}\,\mathrm{Li}_2\left(1-\frac{1}{y}\right) + \frac{3y^2+14y-8}{3(y-1)^4}\ln^2 y + \frac{4y^3-24y^2+2y+6}{3(y-1)^4}\ln y + \frac{-2y^2+13y-7}{(y-1)^3}\right], \tag{B.8}$$

$$W_{8,XY}(y) = \frac{y}{3}\left[\frac{17y^2-25y+36}{2(y-1)^3}\,\mathrm{Li}_2\left(1-\frac{1}{y}\right) - \frac{17y+19}{(y-1)^4}\ln^2 y + \frac{14y^3-12y^2+187y+3}{4(y-1)^4}\ln y - \frac{3(29y^2-44y+143)}{8(y-1)^3}\right], \tag{B.9}$$

$$M_{7,XY}(y) = \frac{2y}{9}\left[\frac{-8y^3+55y^2-68y+21-(6y^2+28y-16)\ln y}{(y-1)^4}\right], \tag{B.10}$$

$$M_{8,XY}(y) = \frac{y}{6}\left[\frac{-7y^3+23y^2-97y+81+(34y+38)\ln y}{(y-1)^4}\right], \tag{B.11}$$

$$T_{7,XY}(y) = \frac{2y}{3}\left[\frac{13y^2-20y+7-(6y^2+4y-4)\ln y}{(y-1)^4}\right], \tag{B.12}$$

$$T_{8,XY} = 2y\left[\frac{-y^2-4y+5+(4y+2)\ln y}{(y-1)^4}\right], \tag{B.13}$$

where $y = m_t^2/M_H^2$.

References

1. G. Buchalla, A.J. Buras, M.E. Lautenbacher, Rev. Mod. Phys. **68**, 1125 (1996)
2. For recent reviews of rare B decays, see T. Hurth, hep-ph/0212304; M. Battaglia et al., hep-ph/0304132
3. S.W. Bosch, G. Buchalla, in Proceedings of the Second Workshop on the CKM Unitarity Triangle, IPPP Duram, April 2003, edited by P. Pall, J. Flynn, P. Kluit, A. Stocchi, eConf C0304052:WG203 (2003)
4. C. Jessop, A world average for $B \to X_s\gamma$, SLAC-PUB-9610
5. K.G. Chetyrkin, M. Misiak, M. Munz, Phys. Lett. B **400**, 206 (1997); **425**, 414(E) (1998)
6. A.L. Kagan, M. Neubert, Eur. Phys. J. C 7, 5 (1999)
7. A.J. Buras, A. Czarnecki, M. Misiak, J. Urban, Nucl. Phys. B **611**, 488 (2001); **631**, 219 (2002), and references therein
8. P. Gambino, M. Misiak, Nucl. Phys. B **611**, 338 (2001)
9. For recent developments see C. Greub, talk presented at the EPS-2003, 17–23 July 2003, Aachen, Germany
10. M. Carena, D. Garcia, U. Nierste, C.E. Wagner, Phys. Lett. B **499**, 141 (2001); G. Degrassi, P. Gambino, G.F. Giudice, JHEP **0012**, 009 (2000); G. D'Ambrosio, G.F. Giudice, G. Isidori, A. Strumia, Nucl. Phys. B **645**, 255 (2002)
11. F. Borzumati, C. Greub, T. Hurth, D. Wyler, Phys. Rev. D **62**, 075005 (2000); T. Besmer, C. Greub, T. Hurth, Nucl. Phys. B **609**, 359 (2001)
12. S. Glashow, S. Weinberg, Phys. Rev. D **15**, 1958 (1977); J.F. Gunion, H.E. Haber, G. Kane, S. Dawson, The Higgs hunter's guide (Addison Wesley, Redwood-City 1990), and references therein
13. Z.J. Xiao, L.B. Guo, Phys. Rev. D **69**, 014002 (2004)
14. CLEO Collaboration, R. Ammer et al., Phys. Rev. Lett. **71**, 674 (1993); T. Coan et al., Phys. Rev. Lett. **84**, 5283 (2000)
15. B. Aubert et al., BaBar Collaboration, Phys. Rev. Lett. **88**, 101805 (2002); hep-ex/0306038
16. K. Abe et al., Belle Collaboration, Measurement of the $B \to K^*\gamma$ branching fraction and asymmetries, Belle-Conf-0319, EPS-ID 537
17. For recent developments, see M. Nakao (for Belle, BaBar, CLEO,VDF and D0 Collaborations), Radiative and electroweak rare B decays, talk presented at LP 2003, August 12, 2003
18. N.G. Deshpande, P. Lo, J. Trampetic, Phys. Rev. Lett. **59**, 183 (1987)
19. C. Greub, H. Simma, D. Wyler, Nucl. Phys. B **434**, 39 (1995) [Erratum B **444**, 447 (1995)]
20. H.H. Asatryan, H.M. Asatrian, D. Wyler, Phys. Lett. B **470**, 223 (1999)
21. H.-n. Li, G.L. Lin, Phys. Rev. D **60**, 054001 (1999)
22. M. Beneke, T. Feldmann, D. Seidel, Nucl. Phys. B **612**, 25 (2001)
23. A. Ali, A.Y. Parkhomenko, Eur. Phys. J. C **23**, 89 (2002)
24. S.W. Bosch, G. Buchalla, Nucl. Phys. B **621**, 459 (2002)
25. M. Beneke, G. Buchalla, M. Neubert, C.T. Sachrajda, Phys. Rev. Lett. **83**, 1914 (1999); Nucl. Phys. B **591**, 313 (2000); Nucl. Phys. B **606**, 245 (2001)
26. S.W. Bosch, Exclusive Radiative Decays of B Mesons in QCD Factorization, Ph.D. thesis, hep-ph/0208203
27. A.L. Kagan, M. Neubert, Phys. Lett. B **539**, 227 (2002)
28. A. Ali, T. Handoko, D. London, Phys. Rev. D **63**, 014014 (2001); A. Ali, E. Lunghi, Eur. Phys. J. C **26**, 195 (2002)
29. M. Kabayashi, T. Maskawa, Prog. Theor. Phys. **49**, 652 (1973)
30. A.J. Buras, M. Misiak, M. Münz, S. Pokorski, Nucl. Phys. B **424**, 374 (1994)
31. Particle Data Group, K. Hagiwara et al., Phys. Rev. D **66**, 010001 (2002) and 2003 partial update for edition 2004 (URL: http://pdg.lbl.gov)
32. P. Ball, V.M. Braun, Phys. Rev. D **58**, 094016 (1998)
33. D. Becirevic, talk given at the Ringberg Phenomenology Workshop on Heavy Flavors, Ringberg Castle, Tegernsee, Germany, May 2003
34. D. Atwood, L. Reina, A. Soni, Phys. Rev. D **55**, 3156 (1997)
35. T.P. Cheng, M. Sher, Phys. Rev. D **35**, 3484 (1987); M. Sher, Y. Yuan, Phys. Rev. D **44**, 1461 (1991); W.S. Hou, Phys. Lett. B **296**, 179 (1992); A. Antaramian, L.J. Hall,

A. Rasin, Phys. Rev. Lett. **69**, 1871 (1992); L.J. Hall, S. Winberg, Phys. Rev. D **48**, R979 (1993); D. Chang, W.S. Hou, W.Y. Keung, Phys. Rev. D **48**, 217 (1993); Y.L. Wu, L. Wolfenstein, Phys. Rev. Lett. **73**, 1762 (1994); D. Atwood, L. Reina, A. Soni, Phys. Rev. Lett. **75**, 3800 (1995)
36. W.S. Hou, R.S. Willey, Phys. Lett. B **202**, 59 (1988); S. Bertolini et al., Nucl. Phys. B **353**, 591 (1991); C.D. Lü, Nucl. Phys. B **441**, 33 (1994)
37. F.M. Borzumati, C. Greub, Phys. Rev. D **58**, 074004 (1998); **59**, 057501 (1999) (Addendum)
38. M. Ciuchini, G. Degrassi, P. Gambino, G.F. Giudice, Nucl. Phys. B **527**, 21 (1998)
39. P. Ciafaloni, A. Romanino, A. Strumia, Nucl. Phys. B **524**, 361 (1998)
40. T.M. Aliev, E.O. Iltan, J. Phys. G **25**, 989 (1999)
41. D.B. Chao, K. Heung, W.Y. Keung, Phys. Rev. D **59**, 115006 (1999)
42. K. Kirs, A. Soni, G.H. Wu, Phys. Rev. D **59**, 096001 (1999); **62**, 116004 (2000); G.H. Wu, A. Soni, Phys. Rev. D **62**, 056005 (2000)
43. Z,J. Xiao, C.S. Li, K.T. Chao, Phys. Rev. D **63**, 074005 (2001); J.J. Cao, Z.J. Xiao, G.R. Lu, Phys. Rev. D **64**, 014012 (2001); D. Zhang, Z.J. Xiao, C.S. Li, Phys. Rev. D **64**, 014014 (2001); Z.J. Xiao, K.T. Chao, C.S. Li, Phys. Rev. D **65**, 114021 (2002)
44. P. Gambino, J. Phys. G **27**, 1199 (2001)
45. M. Gronau, J.L. Rosner, Phys. Lett. B **500**, 247 (2001); M. Gronau, Phys. Lett. B **492**, 297 (2000); T. Hurth, T. Mannel, Phys. Lett. B **511**, 196 (2001); R. Fleischer, Phys. Lett. B **459**, 306 (1999)